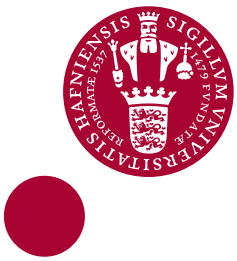

Dysregulated Glial Differentiation in Schizophrenia May Be Relieved by Suppression of SMAD4- and REST-Dependent Signaling

Liu, Zhengshan; Osipovitch, Mikhail; Benraiss, Abdellatif; Huynh, Nguyen P.T.; Foti, Rossana; Bates, Janna; Chandler-Militello, Devin; Findling, Robert L.; Tesar, Paul J.; Nedergaard, Maiken; Windrem, Martha S.; Goldman, Steven A.

Published in:
Cell Reports

DOI:
10.1016/j.celrep.2019.05.088

Publication date:
2019

Document version
Publisher's PDF, also known as Version of record

Article

Cell Reports

Dysregulated Glial Differentiation in Schizophrenia May Be Relieved by Suppression of SMAD4- and REST-Dependent Signaling

Graphical Abstract

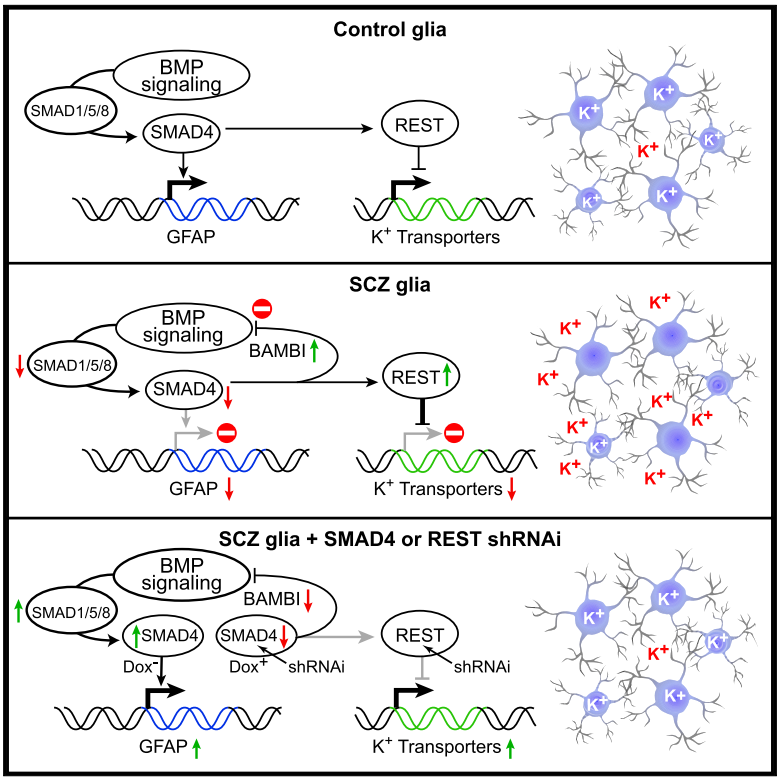

Highlights

- Dysregulated BMP signaling restricts the differentiation of SCZ glial progenitor cells
- REST is regulated by BMP/SMAD4 signaling and is overexpressed by SCZ GPCs
- SMAD4 knockdown rescues normal astrocytic differentiation by SCZ GPCs
- REST knockdown rescues K^+ transporter gene expression and K^+ uptake by SCZ glia

Authors

Zhengshan Liu, Mikhail Osipovitch, Abdellatif Benraiss, ..., Maiken Nedergaard, Martha S. Windrem, Steven A. Goldman

Correspondence

steven_goldman@urmc.rochester.edu, goldman@sund.ku.dk

In Brief

Astrocytic differentiation is impaired in childhood-onset schizophrenia (SCZ). Liu et al. report that SMAD4-dependent BMP signaling and REST are upregulated in hiPSC-derived SCZ glia and that SMAD4 and REST knockdown rescue both astroglial differentiation and K^+ transport. SCZ astrocytic maturation may thus be rescued by targeting SMAD4- and REST-dependent transcription.

Liu et al., 2019, Cell Reports 27, 3832–3843
June 25, 2019
https://doi.org/10.1016/j.celrep.2019.05.088

CellPress

OPEN ACCESS
CellPress

Cell Reports
Article

Dysregulated Glial Differentiation in Schizophrenia May Be Relieved by Suppression of SMAD4- and REST-Dependent Signaling

Zhengshan Liu,[1] Mikhail Osipovitch,[2] Abdellatif Benraiss,[1] Nguyen P.T. Huynh,[1] Rossana Foti,[2] Janna Bates,[1] Devin Chandler-Militello,[1] Robert L. Findling,[3] Paul J. Tesar,[4] Maiken Nedergaard,[1,2] Martha S. Windrem,[1] and Steven A. Goldman[1,2,5,6,*]

[1]Center for Translational Neuromedicine and Department of Neurology, University of Rochester Medical Center, Rochester, NY 14642, USA
[2]Center for Neuroscience, University of Copenhagen Faculty of Health and Medical Sciences, 2200 Copenhagen N, Denmark
[3]Department of Psychiatry, Johns Hopkins Medical School, Baltimore, MD, USA
[4]Department of Genetics, Case Western University Medical School, Cleveland, OH 44106, USA
[5]Neuroscience Center, Rigshospitalet, Copenhagen, Denmark
[6]Lead Contact
*Correspondence: steven_goldman@urmc.rochester.edu or goldman@sund.ku.dk
https://doi.org/10.1016/j.celrep.2019.05.088

SUMMARY

Astrocytic differentiation is developmentally impaired in patients with childhood-onset schizophrenia (SCZ). To determine why, we used genetic gain- and loss-of-function studies to establish the contributions of differentially expressed transcriptional regulators to the defective differentiation of glial progenitor cells (GPCs) produced from SCZ patient-derived induced pluripotent cells (iPSCs). Negative regulators of the bone morphogenetic protein (BMP) pathway were upregulated in SCZ GPCs, including BAMBI, FST, and GREM1, whose overexpression retained SCZ GPCs at the progenitor stage. SMAD4 knockdown (KD) suppressed the production of these BMP inhibitors by SCZ GPCs and rescued normal astrocytic differentiation. In addition, the BMP-regulated transcriptional repressor REST was upregulated in SCZ GPCs, and its KD similarly restored normal glial differentiation. REST KD also rescued potassium-transport-associated gene expression and K^+ uptake, which were otherwise deficient in SCZ glia. These data suggest that the glial differentiation defect in childhood-onset SCZ, and its attendant disruption in K^+ homeostasis, may be rescued by targeting BMP/SMAD4- and REST-dependent transcription.

INTRODUCTION

Schizophrenia (SCZ) affects roughly 1% of the population worldwide and has been the focus of increasingly fruitful efforts to understand its genetic foundations; nonetheless, its cellular basis remains poorly understood (Allen et al., 2008; Sawa and Snyder, 2002). Yet recent reports, including both genome-wide association and differential expression studies, have linked a number of candidate loci as well as specific differentially expressed genes to schizophrenic pathogenesis (Fromer et al., 2016; Marshall et al., 2017; Schizophrenia Working Group of the Psychiatric Genomics Consortium, 2014). Over the past decade in particular, it has become clear that a number of these SCZ-associated genes are involved in the development and physiology of glial cells (Takahashi and Sakurai, 2013; Takahashi et al., 2011a, 2011b; Yin et al., 2012). Accordingly, both astrocytic and oligodendrocytic dysfunction has been implicated in the etiology of SCZ (Aberg et al., 2006; Fields, 2008; Goudriaan et al., 2014; Tkachev et al., 2003; Voineskos et al., 2013; Wang et al., 2015). Astrocytes in particular have essential roles in both the structural development of neural networks as well as the coordination of neural circuit activity, the latter through their release of glial transmitters, maintenance of synaptic density, and regulation of synaptic potassium and neurotransmitter levels (Christopherson et al., 2005; Chung et al., 2013; Rangroo Thrane et al., 2013). As such, defective astrocytic maturation may be an important contributor to the neural circuit disruption characteristic of SCZ (Singh et al., 2016; Verkhratsky and Parpura, 2016; Xia et al., 2016).

To investigate the role of glial pathology in SCZ as well as other neuropsychiatric disorders, we first established a protocol for generating human glial progenitor cells (hGPCs) from patient-derived induced pluripotent cells (iPSCs) (Wang et al., 2013). This protocol permits us to generate hGPCs and their derived astrocytes and oligodendrocytes from patients with SCZ, in a manner that preserves their genetic integrity and functional repertoires. As such, this method has provided us a means by which to assess the differentiation, gene expression, and functional competence of astrocytes derived from patients with SCZ, both *in vitro* and *in vivo*, the latter after engraftment into immunodeficient mice (Windrem et al., 2017). We found that such glial chimeric mice, when neonatally colonized with iPSC-derived hGPCs produced from patients with childhood-onset SCZ, exhibited profound abnormalities in both astrocytic differentiation and structure; these were associated with significant behavioral abnormalities in the engrafted mice relative to controls implanted with normal human hGPCs. Importantly, RNA sequence analysis revealed that the maturational defects in these SCZ hGPCs

were associated with the downregulation of a core set of differentiation-associated genes, whose transcriptional targets included a host of transporters, channels, and synaptic modulators that were themselves deficient in SCZ glia (Windrem et al., 2017).

In the present study, we sought to capitalize upon these findings by identifying targetable signaling nodes at which SCZ-associated glial pathology might be moderated. To that end, we generated iPSC hGPCs from patients with childhood-onset SCZ, or from normal control (CTR) subjects, and then compared both the patterns of gene expression and extent of astrocytic functional differentiation by these cells. We found that excessive bone morphogenetic protein (BMP)-dependent signaling plays a critical role in the disrupted astroglial differentiation of SCZ hGPCs, that BMP's actions in this context are signaled through SMAD4 and mediated in part by a compensatory upregulation of endogenous BMP antagonists, and that aspects of normal phenotype may then be restored to SCZ glia by SMAD4 knockdown (KD). Since the preservation of K^+ homeostasis is a critical element of astrocytic function, and our RNA sequencing (RNA-seq) data indicated the downregulation of a number of potassium channels, pumps, and transporters (hereafter referred to simply as potassium transporters) by SCZ glia, we then assessed the uptake of K^+ by SCZ astrocytes. We found that the SCZ cells indeed manifested significantly impaired K^+ uptake relative to CTR astrocytes and, moreover, that aberrant expression of the REST repressor was responsible for their diminished transcription of the potassium transporter genes. Together, these studies highlight the dysregulation of glial BMP/SMAD4- and REST-dependent transcription as important contributors to the pathogenesis of SCZ and identify these as intriguing new targets for rescuing both glial phenotype and function in this disorder.

RESULTS

Astrocytic Differentiation Was Impaired in SCZ GPCs

iPSCs were produced from skin samples obtained from patients with childhood-onset SCZ, as well as healthy young adult CTRs free of known mental illness, as previously described (Windrem et al., 2017). Patient identifiers were not available to investigators besides the treating psychiatrist, although age, gender, race, diagnosis, and medication history accompanied cell line identifiers. Briefly, fibroblasts were isolated from each sample; from these, 8 human-induced pluripotent stem cell (hiPSC) lines were derived from patient samples and normal CTRs (5 juvenile-onset SCZ patients and 3 healthy gender-matched and age-analogous CTRs; Table S1). iPSCs were generated using excisable floxed polycistronic hSTEMCCA lentivirus (Somers et al., 2010; Zou et al., 2012) encoding Oct4, Sox2, Klf4, and c-Myc (Takahashi et al., 2007; Welstead et al., 2008). A fourth hiPSC CTR line, C27 (Chambers et al., 2009), was also used, to ensure that all genomic and phenotypic data were consistent with prior work in our lab (Wang et al., 2013). All lines were validated as pluripotent using RNA-seq and immunolabeling to assess pluripotent gene expression. The identity of each iPSC line was confirmed to match the parental donor fibroblasts using short tandem repeat (STR)-based DNA fingerprinting, and each line was karyotyped and arrayed for comparative genomic hybridization to confirm genomic integrity. In addition, these iPSC lines were arrayed for genome-wide methylation to compare their methylation state.

We first compared the glial differentiation efficiency of cells derived from SCZ patients and control subjects (n = 4 lines from 4 different patients, each with $\geq$ 3 repeats/patient, each versus paired CTR), by instructing these iPSC cells to GPC fate as previously described (Wang et al., 2013) and assessing their expression of stage-specific markers of maturation as a function of time. We found that all tested iPSCs exhibited typical colonies, and expressed markers of pluripotency by flow cytometry, including SSEA4 (Figure S1A). At the neural progenitor cell (NPC) stage, both immunocytochemistry (ICC) and flow cytometry revealed that the expression levels of the stage-selective markers paired box protein pax-6 (PAX6), sex determining region Y-box 1 (SOX1), and the cell surface marker prominin-1/CD133 were no different between CTR- and SCZ-derived lines (Figures 1A–1D; Figure S1B). At the GPC stage, their expression of the GPC-selective platelet-derived growth factor receptor alpha (PDGFRα/CD140a) (Sim et al., 2011) was then assessed, which revealed that the efficiencies of GPC generation did not differ significantly between SCZ- and CTR-derived NPCs (Figures 1E–1G; Figure S1C). At the astrocytic progenitor stage, the flow cytometry confirmed that the expression levels of cell surface marker CD44 were no different between CTR- and SCZ-derived lines (Figure S1D). Thus, no differences in the differentiation of SCZ and CTR iPSCs were noted through the GPC and astrocytic progenitor stages.

At that point, the SCZ- and CTR-derived GPCs were further differentiated into astrocytes by incubating in M41 medium supplemented with 20 ng/ml BMP4 for 4 weeks. Immunolabeling revealed that the proportion of $GFAP^+$ astrocytes was significantly higher in CTR lines (4 CTR lines, n $\geq$ 3 per line, mean of 4 CTR lines = 70.1% $\pm$ 2.4%) than in SCZ lines (4 SCZ lines, n $\geq$ 3 per line, mean of 4 SCZ lines = 39.9% $\pm$ 2.0%; $p < 0.001$, two-tailed t test) (Figures 1H–1J). In addition to GFAP, the percentage of $S100\beta^+$ astrocytes was also significantly higher in CTR lines relative to SCZ lines (Figure S1F). In contrast, the proportion of $PDGF\alpha R^+$ GPCs was significantly higher in BMP4-treated SCZ glia (4 SCZ lines, n $\geq$ 3 per line) relative to BMP4-treated CTR glia (4 CTR lines, n $\geq$ 3 per line) (Figure S1E). This defect of astrocytic differentiation was consistently observed in all SCZ GPCs relative to CTR cells and comprised an *in vitro* correlate to previously described astroglial differentiation defects *in vivo* (Windrem et al., 2017).

SCZ GPCs Upregulated Expression of BAMBI, an Inhibitor of BMP Signaling

To identify the molecular concomitants to the defective astrocytic differentiation of SCZ GPCs, we had earlier performed RNA-seq on fluorescence-activated cell sorting (FACS)-sorted $CD140a^+$ GPCs from 3 different CTR- and 4 SCZ-derived lines at time points ranging from 154 to 242 days *in vitro* (Windrem et al., 2017). mRNA was isolated from these cells with polyA-selection for RNA-seq on an Illumina HiSeq 2500 platform for approximately 45 million 1x100 bp reads per sample. The original counts were analyzed to determine disease-dysregulated

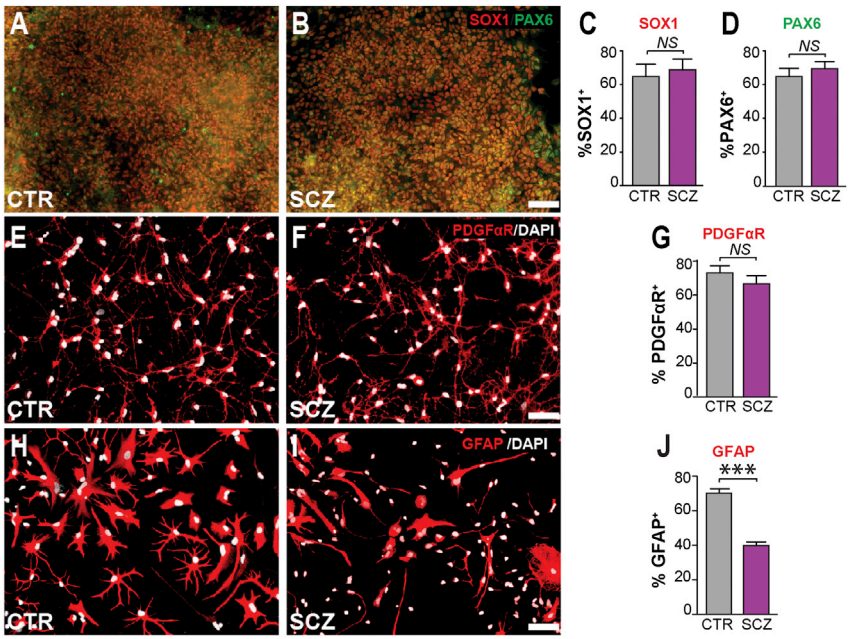

Figure 1. Astrocytic Differentiation Was Impaired in SCZ GPCs

(A–D) At the neural progenitor cell (NPC) stage, both CTR (A) and SCZ (B) hNPCs (representative examples of lines derived from 4 distinct patients, n ≥ 3/each line) highly expressed both SOX1 (C) and PAX6 (D).

(E–G) Similarly, the efficiency of PDGFRα/CD140a-defined hGPC generation (G) did not differ between CTR (E) and SCZ (F) lines (4 different patient-specific lines each, n ≥ 3/each line).

(H–J) In contrast, the proportion of GFAP$^+$ astrocytes (J) was significantly higher in CTR cultures (H; 4 CTR lines, n ≥ 3/each line [70.1% ± 2.4%]) than in identically raised SCZ cultures (I; 4 SCZ lines, n ≥ 3/each line [39.9% ± 2.0%]).

Scale: 50 μm; ***p < 0.001 by two-tailed t test; *NS*, not significant; mean ± SEM.

genes at 5% false discovery rate (FDR) and log2 fold change > 1. By that means, we had identified 118 mRNAs that were consistently and significantly differentially expressed by CD140a-sorted SCZ hGPCs relative to their CTR iPSC hGPCs (Windrem et al., 2017). Among these, a number of genes involved in glial lineage progression were downregulated in SCZ hGPCs relative to their normal CTRs, suggesting that astroglial differentiation was impaired in SCZ in a cell-autonomous fashion, due to intrinsic defects in SCZ-derived GPCs.

Capitalizing upon these earlier data, in this study we first used Ingenuity Pathway Analysis (IPA) to identify pathways that were significantly differentially regulated in SCZ hGPCs. We found that among these, BMP-signaling-related transcripts were upregulated in SCZ hGPCs compared to CTR hGPCs (Figure S2A). qPCR then validated that the expression of a number of transforming growth factor β (TGF-β) pathway regulators, including BAMBI, was indeed significantly elevated in SCZ GPCs (Figure S2B). In contrast, these BMP-signaling-related transcripts did not differ between SCZ and CTR lines at the NPC stage (Figure S2C). Moreover, the methylation states of CTR- and SCZ-derived iPSCs were similar (Figure S2D); the little variability noted across lines in iPSC methylation state appeared due to sex and line but not to disease state or subject age (Figure S2E). Thus, the upregulation of BAMBI and other TGF-β and BMP pathway regulators that we noted in SCZ hGPCs was not due to any systematic, disease-dependent difference in methylation pattern between CTR and SCZ cells at the pluripotent stem cell stage.

BMP4 is a strong stimulus for astrocytic differentiation by hGPCs, and BAMBI is a strong antagonist to BMP4-induced glial induction, acting as a pseudo-receptor and hence dominant-negative inhibitor of BMP signaling (Sim et al., 2006). Yet BAMBI expression may be activated by TGF-β- and BMP-receptor-dependent signaling as a compensatory negative feedback response (Onichtchouk et al., 1999). Accordingly, our RNA-seq, qPCR data revealed that both BMP-signaling-dependent transcripts and BAMBI were upregulated in SCZ hGPCs but not in SCZ human NPCs (hNPCs) (Figures S2B and S2C). These data suggest that the upregulation of BMP signaling was specific to SCZ glia and first appeared at the glial progenitor stage and that this process was associated with the upregulated expression of BAMBI, which in turn suppressed the astrocytic differentiation of SCZ hGPCs.

On that basis, we asked whether BAMBI overexpression in hGPCs derived from normal CTR subjects might mimic or reproduce the SCZ GPC phenotype by suppressing the differentiation of these hGPCs. To that end, we genetically modulated the expression of BAMBI in hGPCs, both SCZ and CTR-derived GPCs (Figure S3). We found that overexpression of BAMBI in CTR GPCs significantly decreased their efficiency of astrocytic transition (4 CTR lines with 3 repeats/each line, mean of 4 CTR lines/36.4% ± 4.3%), yielding cells that resembled SCZ hGPCs in their refractoriness to terminal astrocytic maturation (4 SCZ lines with 3 repeats/each line, mean of 4 SCZ lines/45.5% ± 3.6%; p = 0.12 by two-tailed t test) (Figures 2A and 2B). However, BAMBI KD in SCZ GPCs did not rescue astrocytic differentiation in the latter, suggesting that BAMBI overexpression contributed to the resistance of SCZ hGPCs to maturation but was not sufficient in this regard (Figures 2A and 2B). Accordingly, when we used qPCR to assess the expression of alternative inhibitors of BMP signaling, we found that the mRNAs encoding both follistatin (FST) and gremlin1 (GREM1), two potent antagonists of BMPs and BMP-dependent signaling, were both significantly upregulated by SCZ GPCs (SCZ versus CTR; 4 SCZ and 4 CTR lines, 3 repeats/each line; delta-delta-Ct [ddCt] of FST = 2.45 ± 0.39, p < 0.05; GREM1 = 3.38 ± 0.53, p < 0.01; two-tailed t test) (Figure 2C).

Astrocytic Differentiation by SCZ GPCs May Be Rescued by SMAD4 KD

SMAD4 is necessary for canonical BMP signaling in that it acts as a common effector for multiple upstream signals, in response to which it translocates to the nucleus, where it activates both

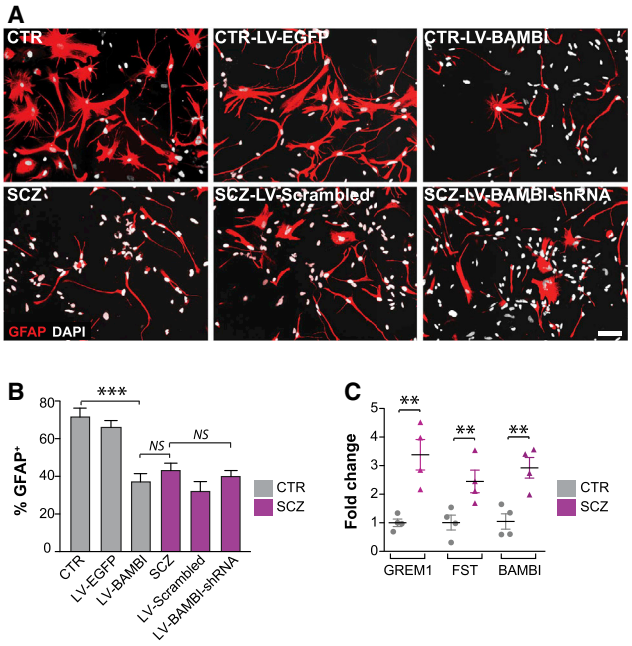

Figure 2. BAMBI Expression in Normal hGPCs Phenocopied the Glial Differentiation Defect of SCZ

(A) Upper panel: lentiviral (LV) overexpression of the membrane-bound BMP antagonist BAMBI in CTR hGPCs (CTR-LV-BAMBI) 4 CTR lines, 3 repeats/each line) significantly decreased their efficiency of astrocytic transition (4 CTR lines, 3 repeats/each line). Lower panel: however, BAMBI knockdown (KD) in SCZ hGPCs was not sufficient to restore astrocytic differentiation (4 SCZ lines, 3 repeats/each line).

(B) Quantification of the proportion of GFAP-expressing astrocytes confirmed that BAMBI overexpression suppressed the efficiency of astrocytic differentiation of CTR hGPCs to a level indistinguishable from that of SCZ hGPCs, while BAMBI KD in SCZ hGPCs was not sufficient to rescue astrocytic differentiation to control levels.

(C) Besides BAMBI, the BMP antagonists follistatin (FST) and gremlin1 (GREM1) were also upregulated in SCZ hGPCs relative to controls.

Scale: 50 μm; ***$p < 0.001$, one-way ANOVA for (B); **$p < 0.001$ by two-tailed t test for (C); *NS*: not significant; mean ± SEM.

BMP- and TGF-β-regulated genes (Herhaus and Sapkota, 2014). These include BAMBI as well as FST and GREM1, all acting in concert as negative feedback regulators of pro-gliogenic BMP signals (Brazil et al., 2015; Onichtchouk et al., 1999) (Figure 3A). On that basis, we posited that SMAD4 KD in hGPCs, by inhibiting the early expression of BAMBI, FST, and GREM1, might potentiate astrocytic differentiation from hGPCs. Furthermore, to the extent that the differentiation block in SCZ hGPCs was due to the SMAD4-mediated overexpression of endogenous BMP inhibitors, we postulated that SMAD4 KD would therefore differentially potentiate astroglial differentiation by SCZ hGPCs. To test this possibility, we used doxycycline (DOX) induction of SMAD4 short hammerhead RNA interference (shRNAi) to conditionally KD SMAD4 expression in both SCZ and CTR hGPCs and then assessed their expression of BMP-regulated genes by qPCR (Figures S4A–S4C). We found that SMAD4 KD indeed repressed the expression of BMP-signaling-dependent genes, including BAMBI, FST, and GREM1 (SCZ-LV-Scrambled versus SCZ-LV-SMAD4-shRNA; 4 different patient iPSC lines/group, 3 repeats/line; ddCt of BAMBI: 2.56 ± 0.35, $p < 0.05$; FST: 2.38 ± 0.24, $p < 0.01$; GREM1: 3.04 ± 0.45, $p < 0.05$; all comparisons by ANOVA with post hoc t tests) (Figure 3B). Importantly, transient DOX-induced SMAD4 KD, in which shRNAi expression was limited to the progenitor stage, robustly promoted the astrocytic differentiation of the SCZ GPCs, overcoming their relative block in glial differentiation to effectively rescue astrocytic phenotype (Figures 3C and 3D). In particular, SMAD4 KD in SCZ GPCs restored their efficiency of GFAP-defined astrocytic differentiation to that of CTR GPCs (SCZ-SMAD4-shRNA at the GPC stage: 56.8% ± 3.8%; CTR lines: 62.2% ± 4.0%; $p > 0.05$, one-way ANOVA; mean ± SE of 4 distinct patient lines/group, $n \geq 3$ replicates/line) (Figures 3C and 3D). In contrast, continuous SMAD4 KD *after* astrocytic induction, as mediated via continuous DOX exposure (as outlined in Figure S4B), caused a diminution of GFAP-defined astrocytes in both SCZ and CTR groups (Figures 3C and 3D). Thus, maintenance of mature astrocytic phenotype appeared to require ongoing SMAD4 signaling in SCZ and CTR astrocytes alike.

Together, these data indicate that aberrant BMP signaling in SCZ GPCs, by driving the excessive expression of inhibitors of BMP signaling, suppresses astrocytic differentiation and that this differentiation defect can be rescued by SMAD4 KD. Nonetheless, once SCZ GPCs have progressed to astrocytic differentiation, SMAD4 expression is then required for maintenance of the astrocytic phenotype in CTR and SCZ astrocytes alike, consistent with its previously described function as the effector of BMP-mediated astrocytic maturation (Kohyama et al., 2010). These data indicate that pathological BMP-dependent signaling in SCZ GPCs may delimit their astrocytic maturation and suggest that this cellular pathology may arise in part from the SMAD4-dependent overexpression of endogenous inhibitors of pro-gliogenic BMP signaling by GPCs.

SCZ Astrocytes Exhibit Reduced Potassium Uptake

Together with the impaired astrocytic differentiation of SCZ GPCs, our RNA-seq data suggested that those astrocytes that do successfully differentiate might nonetheless be functionally impaired. In particular, the RNA-seq revealed the downregulated transcription in SCZ GPCs of a broad set of potassium channel (KCN)-encoding genes, including the Na^+-K^+ ATPase, Na^+-K^+/$2Cl^-$ cotransporter (NKCC), and Kir-family inwardly rectifying KCNs (Figure 4A) (Windrem et al., 2017), all of which play important roles in potassium uptake by astrocytes (Larsen et al., 2014; Macaulay and Zeuthen, 2012) (Figure 5A). Among these dysregulated KCN genes, ATP1A2, SLC12A6, and KCNJ9, which respectively encode the Na^+/K^+-ATPase pump, NKCC1 Na^+/K^+/$2Cl^-$ cotransporter, and the Kir3.3 voltage-gated K^+ channel (Bøttger et al., 2016; Gamba and Friedman, 2009; Lesage et al., 1995), were substantially downregulated in SCZ lines compared to the 4 CTR lines; these findings suggested a broad-based impairment of K^+ uptake by SCZ glia.

On the basis of these genomic data, we next asked whether K^+ uptake was actually impaired in SCZ astrocytes. To address this hypothesis, we first used qPCR to confirm whether these K^+ channel-associated genes were dysregulated in SCZ glia. They were indeed significantly downregulated, thus validating the RNA-seq analysis (Figures 4B and 5B). We next assessed

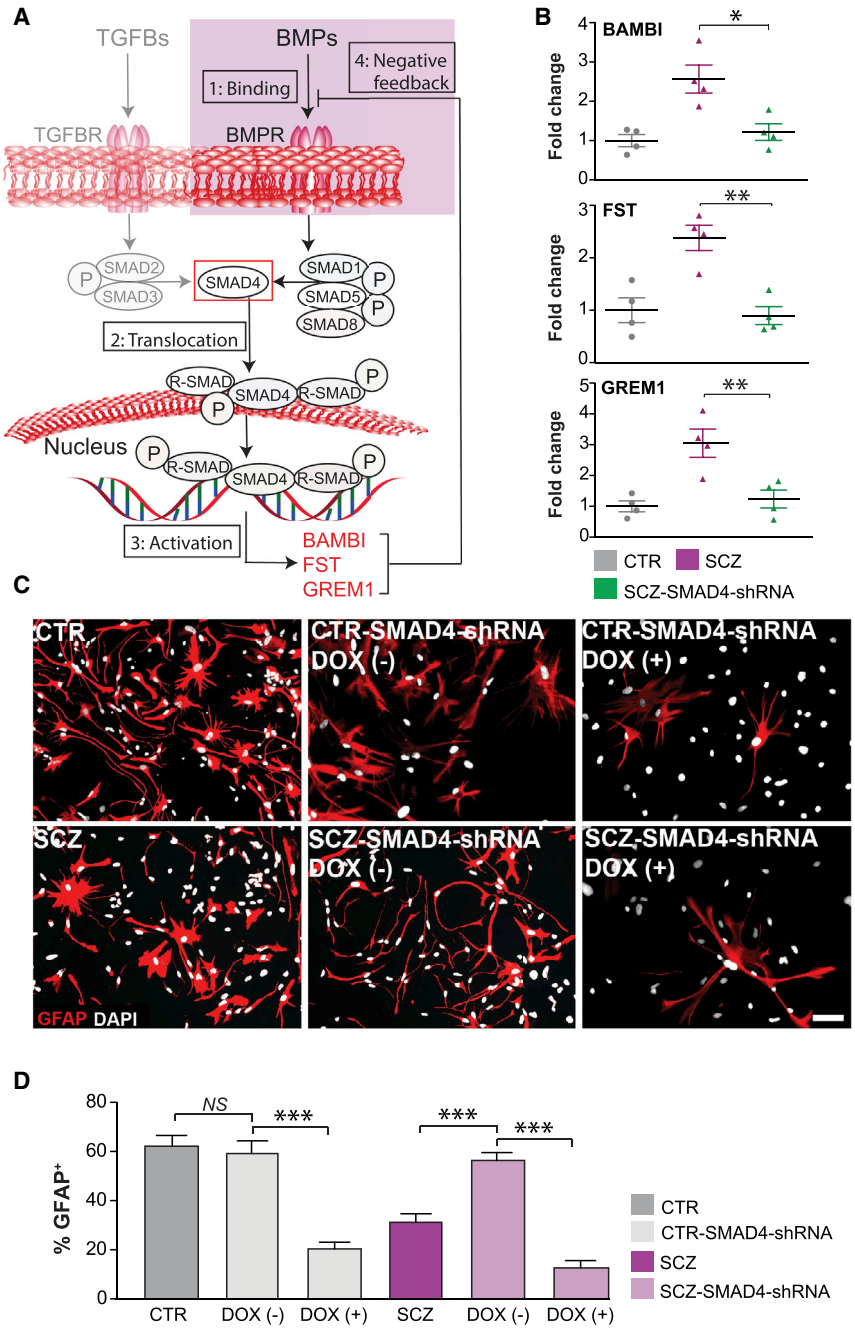

Figure 3. SMAD4 Regulated the Astrocytic Differentiation of SCZ GPCs

(A) SMAD4 regulates the expression of TGF-β and BMP pathway signaling through (1) phosphorylation of both SMAD2/3 and SMAD1/5/8; (2) SMAD nuclear translocation and activation of target promoters, including the early induction of the endogenous BMP inhibitors BAMBI, follistatin (FST), and gremlin1 (GREM1); and (3) their subsequent feedback inhibition of BMP signals.

(B) BAMBI, FST, and GREM1 were all significantly overexpressed in SCZ CD140a-sorted hGPCs relative to control-derived hGPCs. SMAD4 KD in SCZ hGPCs (4 SCZ lines, 3 repeats/line) then repressed the expression of BAMBI, FST, and GREM1 to control levels.

(C) SMAD4 KD in SCZ hGPCs restored astrocytic differentiation to that of CTR hGPCs (4 SCZ lines, 3 repeats/each line). DOX (−)/(+) means short-term/long-term culture with DOX.

(D) SMAD4 KD after astrocytic induction, as mediated via continuous doxycycline exposure, caused a loss of GFAP-defined astrocytes in both SCZ and CTR groups. DOX (−)/(+) means short-term/long-term culture with DOX.

Scale: 50 μm; *$p < 0.05$, **$p < 0.01$, ***$p < 0.001$; one-way ANOVA; *NS*: not significant; mean ± SEM.

functional K^+ uptake directly in cultured SCZ- and CTR-derived astrocytes. To obtain mature SCZ and CTR astrocyte cultures, CD44-sorted glial progenitors were cultured in base media supplemented with 10% fetal bovine serum (FBS) and 20 ng/ml BMP4 for 4 weeks, so as to potentiate the differentiation of mature, glial fibrillary acidic protein (GFAP)-expressing, fiber-bearing astrocytes (Figure S5). Under these highly astrogliogenic conditions, and using cells already sorted for the early astrocytic marker CD44, astrocytic maturation was achieved by both SCZ- and CTR-derived progenitors (Figure S5). Astrocytes from 4 different SCZ and 4 different CTR lines were then incubated with ^{86}Rb, a surrogate monovalent cation for K^+ uptake (Larsen et al., 2014), and rubidium uptake measured as a function of both cell number and total protein. We found the K^+ uptake in SCZ glia (4 SCZ cell lines, 5 repeats/each line) was sharply decreased relative to CTR glia (4 CTR cell lines, 5 repeats/each line), normalized by both cell number and total protein (Figure 5C; $p < 0.001$ by two-tailed t test).

Since genes encoding different potassium Na^+/K^+-ATPase pumps, transporters, and inwardly rectifying channels were dysregulated in SCZ glia, the drugs ouabain, bumetanide, and tertiapin were used to respectively block these three K^+ uptake mechanisms. We first tested different concentrations of each drug to determine its optimal dose range for modulating human astroglial K^+ uptake. We found that ouabain and bumetanide, respectively targeting the Na^+/K^+-ATPase pump and NKCC1-encoded $Na^+/K^+/2Cl^-$ cotransporter, significantly inhibited K^+ uptake in CTR glia, while tertiapin, which targets K_{ir} channels, did not (Figures 5D and 5E). In marked contrast, neither ouabain nor bumetanide affected K^+ uptake by SCZ astrocytes (Figures 5D and 5E). This suggests that the functional decrement in K^+ uptake by SCZ-derived astrocytes may be primarily due to downregulated Na^+/K^+-ATPase and $Na^+/K^+/2Cl^-$ cotransporter function, rendering these cells refractory to ouabain and bumetanide treatment.

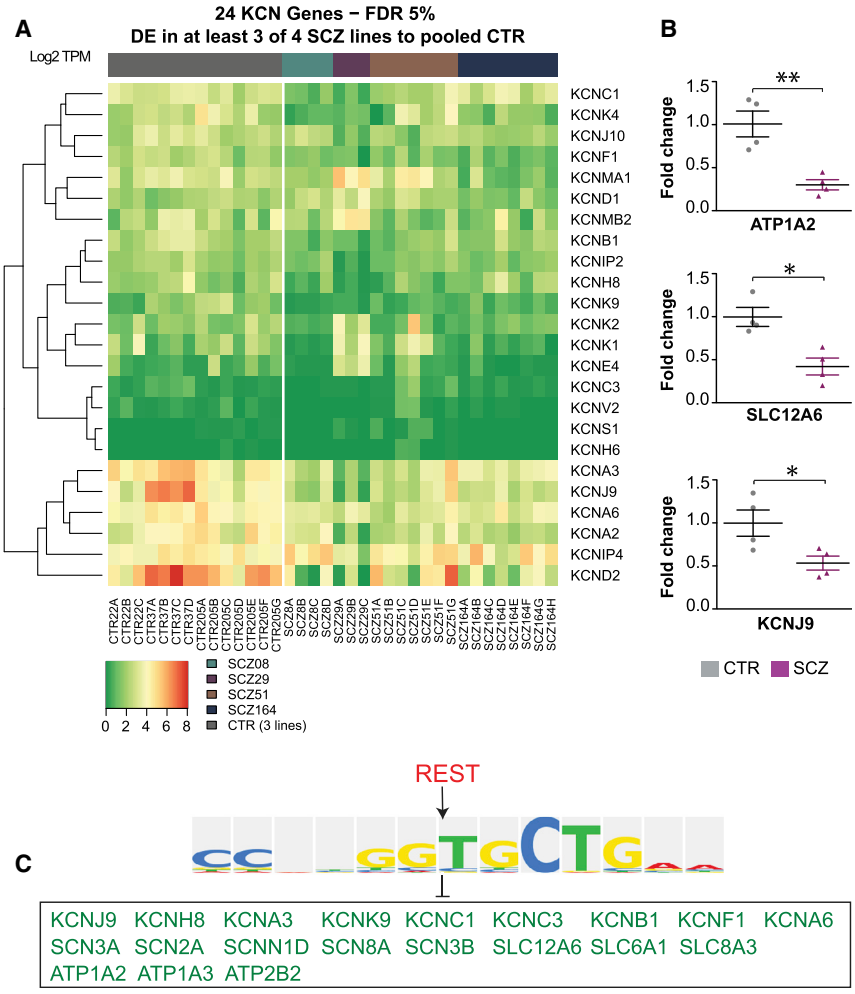

Figure 4. REST Represses KCN-Associated Gene Expression in SCZ hGPCs

(A) Differentially expressed potassium channel genes in SCZ-derived hGPC lines. Each SCZ-derived hGPC line was individually compared against three pooled CTR-derived hGPC lines (FDR 5%, fold change [FC] > 2.00 [if applicable]). Genes shown were found differentially expressed in at least three out of four assessed SCZ-derived hGPC lines.

(B) qPCR confirmed that potassium-channel-associated genes including ATP1A2, SLC12A6, and KCNJ9 were all significantly downregulated in SCZ hGPCs (4 SCZ lines, 3 repeats/each line) relative to CTR cells (4 CTR lines, 3 repeats/each line).

(C) Biobase-Transfac revealed that the majority of downregulated potassium-channel-associated genes in SCZ hGPCs from our RNA-seq data were targets of the REST repressor.

**p < 0.01 by two-tailed t test; mean ± SEM.

REST Regulates Potassium Uptake by SCZ Astrocytes

Since a large number of potassium-channel-encoding genes are dysregulated in SCZ glia, it is difficult to modulate glial K^+ uptake through genetic means targeting individual KCNs alone. To address this issue, we used Biobase-Transfac analysis, which was developed to identify regulatory regions common to different genes, as a means of defining their shared upstream regulators (Hu et al., 2014). By this means, we attempted to pinpoint shared regulatory elements within 1 kb of the transcription start sites (TSSs) of the SCZ-associated glial genes in our datasets; our intent was to identify upstream transcription factors able to modulate these genes as a group. Using a 13 nucleotide consensus sequence (CCNNGGTGCTGAA), we determined that the majority of all downregulated KCN genes were targets of the neuron restrictive silencing factor (NRSF) REST (Figure 4C), a potent transcriptional repressor that acts in neural cells to repress non-neural gene expression (Hirabayashi and Gotoh, 2010). REST levels are relatively high in rodent oligodendrocyte progenitor cells and rise with terminal oligodendroglial maturation (Dewald et al., 2011); similarly, REST levels rise with astrocytic differentiation from uncommitted NPCs (Kohyama et al., 2010). Importantly, REST transcription may be positively modulated by SMAD1/5/8 through BMP signaling (Kohyama et al., 2010), such that the pathologically upregulated BMP signaling we observed in SCZ hGPCs might be expected to drive similarly high levels of REST. On that basis, we queried our RNA-seq data, which confirmed that REST was indeed significantly upregulated in SCZ GPCs relative to CTR GPCs (Windrem et al., 2017). We then used qPCR to confirm that the upregulation of REST expression by SCZ glia was consistent across all of the patients in our series (Figure 6A). Interestingly, while REST levels have been previously linked to terminal glial differentiation (Kohyama et al., 2010), the SCZ hGPCs we evaluated were decidedly refractory to glial differentiation, whether as astrocytes or oligodendrocytes, and this observation was consistent across all patient samples assessed. Thus, the disease context informed the cellular response to REST activity.

On the basis of these data, we postulated that the upregulation of REST in SCZ-derived glia, and their attendant epigenetic modification, might be sufficient to repress potassium-transporter- and channel-associated gene expression. To test this hypothesis, we used lentivirus to overexpress REST in CTR glial cells and assessed K^+ uptake by the transduced cells. In parallel, we knocked down REST expression in SCZ glia through lentiviral shRNAi transduction and then similarly assessed K^+ uptake by these cells. qPCR validation confirmed that REST was significantly modulated as intended in both CTR and SCZ glial cells (Figure S6A). By this means, we found that in both CTR and SCZ glia subjected to REST *over*expression, that the expression of a number of K^+ transport genes, including SLC12A6, KCNJ9, and ATP1A2, was indeed significantly repressed (Figure 6B and 6C). In contrast, the expression of these genes was strongly upregulated in both CTR and SCZ cells subjected to REST KD (Figures 6B and 6C). In addition,

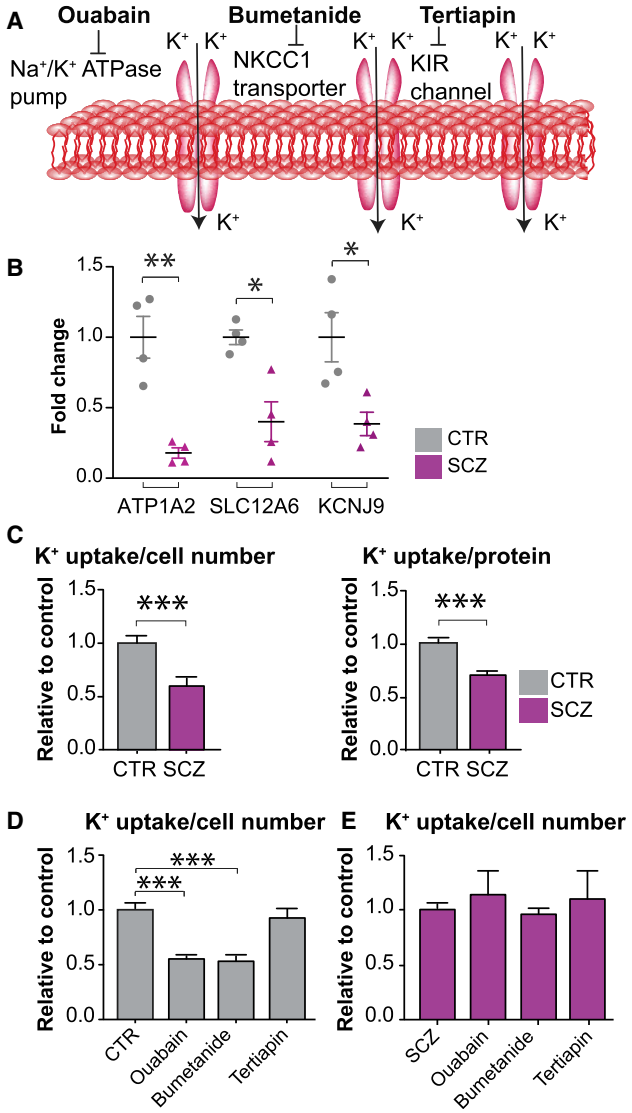

Figure 5. Potassium Uptake Was Decreased by SCZ Astrocytes

(A) The Na^+/K^+-ATPase pump, NKCC1 $Na^+/K^+/2Cl^-$ cotransporter, and inwardly rectifying K^+ channels are all involved in the regulation of potassium uptake by astrocytes.

(B) qPCR confirmed that several K^+-channel-associated genes were downregulated in SCZ $CD44^+$ astrocyte-biased GPCs relative to CTR cells.

(C) SCZ and CTR $CD44^+$ GPCs were cultured in FBS with BMP4 to produce mature $GFAP^+$ astrocytes, which were then assessed for K^+ uptake; the results were normalized to both total protein and cell number. K^+ uptake by SCZ astrocytes was significantly reduced (4 SCZ lines, 5 repeats/each line) compared to K^+ uptake by CTR astrocytes (4 CTR lines, 5 repeats/each line).

(D and E) Astrocytes were treated with ouabain, bumetanide, and tertiapin to assess which potassium transporter classes were functionally impaired in SCZ astrocytes relative to control (4 lines of each, 4 repeats/line). Both ouabain and bumetanide efficiently decreased K^+ uptake by CTR astrocytes (D, gray bars), whereas neither affected K^+ uptake by SCZ astrocytes (E, purple bars).

$^*p < 0.05$, $^{**}p < 0.01$, $^{***}p < 0.001$ by two-tailed t test for (B) and (C); $^{***}p < 0.001$ by one-way ANOVA for (D); *NS*: not significant; mean ± SEM.

we next found that BMP4 treatment of CTR GPCs significantly upregulated REST expression and downregulated K^+ transport gene expression relative to untreated cells, which was restored with BMP signaling inhibitor DMH1 (Figure S6B), and that lentiviral-SMAD4-shRNAi transduction of SCZ GPCs robustly repressed REST expression and enhanced K^+ transport gene expression (Figure S6C).

Importantly, we noted that REST-overexpressing CTR astrocytes mimicked the functional potassium dysregulation of SCZ glia, in that their K^+ uptake was significantly reduced compared to that of untreated CTR glia (Figure 6D). Neither ouabain nor bumetanide further decreased K^+ uptake by these cells, suggesting that their targeted pumps and transporters were downregulated to the point of functional irrelevance (Figure 6E). Conversely, K^+ uptake by SCZ astrocytes subjected to REST KD was strongly increased to levels no different from those of CTR astrocytes (Figure 6D); both ouabain and bumetanide were then able to significantly reduce K^+ uptake by these REST shRNAi-transduced SCZ astrocytes (Figure 6F). Together, these data suggest that REST KD in SCZ glia promoted the restoration of normal K^+ uptake by these cells by rescuing their expression of both Na^+/K^+-ATPase and the NKCC1 $Na^+/K^+/2Cl^-$ cotransporter, thereby restoring a salient feature of astroglial potassium homeostasis (Figure 6G). As such, these observations indicate that REST operates to suppress K^+ uptake by SCZ glia by broadly suppressing the expression and hence function of multiple mechanisms of glial potassium transport.

DISCUSSION

Our data indicate that astrocytic differentiation is impaired in GPCs derived from childhood-onset schizophrenics and that this maturational defect may be rescued by the suppression of either BMP signaling via SMAD4 KD or by the de-repression of glial-differentiation-associated transcription via REST KD. Importantly, astrocytic depletion has been recently noted in both cortical and subcortical regions of patients with SCZ, and this might be especially prominent in the white matter (Rajkowska et al., 2002; Steffek et al., 2008; Williams et al., 2013). Astrocytes play key contributions to neural circuit formation and stability (Christopherson et al., 2005; Clarke and Barres, 2013). Thus, any such developmental defect of astrocytic differentiation in SCZ GPCs might lead to profound defects in the initial formation or stability of neural circuits, a defect that is one of the hallmarks of SCZ (Penzes et al., 2011). In this regard, our RNA-seq data suggested upregulated TGFBR and BMP signaling in SCZ GPCs, which was associated with the activation of downstream BMP-regulated genes that included BAMBI, a competitive inhibitor of pro-gliogenic BMP signaling (Onichtchouk et al., 1999). We have previously noted that high expression of BAMBI in adult hGPCs significantly inhibits their astrocytic differentiation as induced by BMP4 (Sim et al., 2006), suggesting that the pathological elevation of BMP-signaling-induced BAMBI expression in SCZ hGPCs, relative to normal CTR hGPCs, might be sufficient to suppress their differentiation as mature astrocytes. Besides BAMBI, several other inhibitors of TGF-β/BMP signaling, including FST and GREM1 (Brazil et al., 2015), were also

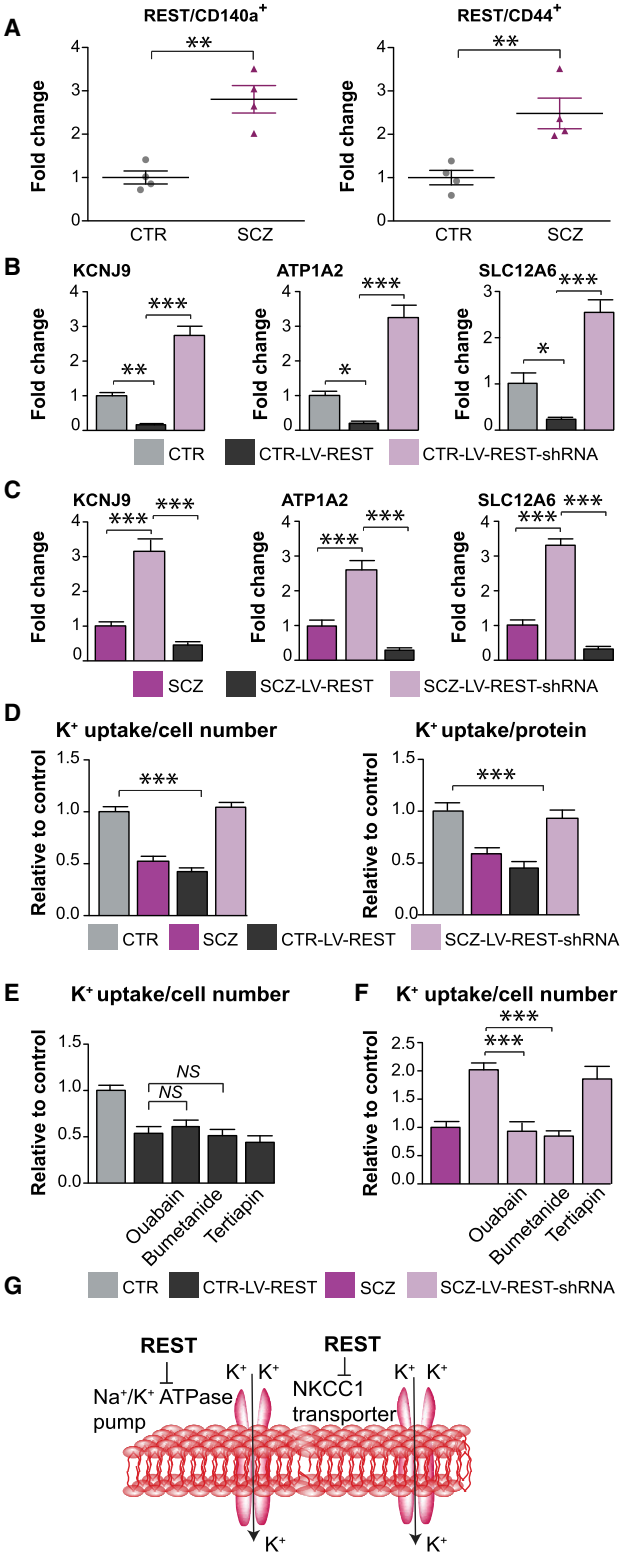

Figure 6. REST KD Restored Potassium Uptake by SCZ Astrocytes

(A) qPCR confirmed that REST was upregulated in both CD140a-sorted SCZ hGPCs relative to their controls and in CD44-sorted SCZ astrocytic progenitor cells relative to CTR cells.

(B and C) The expression of several K^+-transport-associated genes, including SLC12A6, KCNJ9, and ATP1A2, was significantly repressed in both CTR (B) and SCZ (C) glia in which REST was overexpressed via lentiviral-REST transduction (black bars). In contrast, their expression was robustly upregulated in CTR (B) and SCZ (C) cultures in which REST was knocked down via lentiviral-REST shRNAi transduction (purple bars, 4 CTR and SCZ lines, 3 repeats/each line).

(D) K^+ uptake by REST-transduced CTR astrocytes fell, mimicking that SCZ glia, whereas K^+ uptake was rescued in SCZ lines subjected to REST KD.

(E and F) In cultures of CTR glia (E), lentiviral overexpression of REST suppressed K^+ uptake, which was not affected by treatment with ouabain or bumetanide. In contrast, potassium uptake was restored in SCZ glia subjected to REST KD and this rescue was reversed by both ouabain and bumetanide (F) (4 CTR and SCZ lines, 3 repeats/each line).

(G) These data indicate that upregulated REST in SCZ glia may decrease K^+ uptake in part by suppressing the expression and function of the Na^+/K^+-ATPase pump and NKCC1 transporter.

$^{**}p < 0.01$ by two-tailed t test for (A); $^{*}p < 0.05$, $^{**}p < 0.01$, $^{***}p < 0.001$ by one-way ANOVA for (B)–(F); *NS*: not significant; mean ± SEM.

upregulated by SCZ GPCs; these may have permitted SCZ hGPCs to avoid astrocytic fate even after BAMBI KD.

Of note, the activation of canonical TGF-β signaling is dependent upon either SMAD2/3 activation via the TGF-β pathway or SMAD1/5/8 via BMP-receptor-dependent signals; each of these effectors needs to combine with SMAD4 for nuclear translocation prior to the activation of their downstream genetic targets (Hata and Chen, 2016; Herhaus and Sapkota, 2014). Accordingly, we found that SMAD4 KD efficiently suppressed BMP-signaling-induced expression of endogenous BMP inhibitors and by so doing robustly promoted the astrocytic differentiation of otherwise differentiation-resistant SCZ GPCs. Importantly, this differentiative response of hGPCs to SMAD4 inhibition was only noted at the hGPC stage and only in SCZ hGPCs; CTR-patient-derived hGPCs showed no such potentiated differentiation in response to SMAD4 suppression. Thus, the modulation of SMAD4 might represent an appropriate strategy toward relieving the glial differentiation defect in SCZ.

Glial maturation is precisely regulated in human brain development (Goldman and Kuypers, 2015; Molofsky et al., 2012). Astrocytes have a multitude of roles in the CNS, including energy support to both neurons and oligodendrocytes, potassium buffering, neurotransmitter recycling, and synapse formation and maturation; as such, astrocytes play critical roles in neural circuit formation and maintenance (Blanco-Suárez et al., 2017; Clarke and Barres, 2013; Verkhratsky et al., 2015). Astrocytes also contribute to the glymphatic system through the regulation of cerebral spinal fluid flow through the brain interstitium (Xie et al., 2013). Thus, the delayed differentiation of SCZ astrocytes may have significant effects on neural network formation, organization, and mature function alike.

We found that a number of potassium transporters were downregulated in SCZ glia. Interestingly, prior genome-wide association studies (GWASs) have identified an association of potassium pump, transport, and channel genes with SCZ. For instance, the chromosome 1q21-q22 locus, containing KCNN3, has a significant linkage to familial SCZ (Brzustowicz et al., 2000). KCNN3 is widely expressed in the human brain and selectively regulates neuronal excitability and neurotransmitter release in monoaminergic neurons (O'Donovan and

Owen, 1999). In addition to KCNN3, a number of other KCN genes have been associated with SCZ, including KCNQ2 and KCNAB1 (Lee et al., 2013). More recently, a novel *de novo* mutation in ATP1A3, a subunit of the sodium-potassium pump, has been specifically associated with childhood-onset SCZ (Smedemark-Margulies et al., 2016).

The downregulation or dysfunction of these potassium transporters in GPCs and their derived astrocytes may contribute significantly to disease phenotype in SCZ. KCN, pump, and transport genes are widely expressed in both GPCs (Coppi et al., 2013; Maldonado et al., 2013) and astrocytes (Larsen et al., 2014; Zhang and Barres, 2010), in which they regulate not only proliferation, migration, and differentiation but also the relationship of glia to neurons (Coppi et al., 2013; Maldonado et al., 2013). In regards to the latter, astrocytes also regulate synaptic K^+ uptake through all three major K^+ transport mechanisms, including the Na^+/K^+-ATPase, the NKCC1 cotransporter, and inwardly rectifying K_{ir} channels (Larsen et al., 2014; Zhang and Barres, 2010), thereby establishing neuronal firing thresholds over broad regional domains.

Accordingly, dysregulated K^+ transport and KCN gene expression have been associated with a broad variety of neurological and psychiatric diseases. Several K_{ir} genes, including $K_{ir}4.1$, are involved in astrocytic potassium buffering and glutamate uptake, and deletion of these genes has been noted in both Huntington's disease and multiple sclerosis (Seifert et al., 2006; Tong et al., 2014). In addition, mutation of astrocytic ATP1A2, the $\alpha 2$-isoform of the sodium-potassium pump, may be causally associated with familial hemiplegic migraine (Bøttger et al., 2016; Swarts et al., 2013). In all of these examples, glial K^+ uptake is impaired, just as in SCZ glia, and all are associated with elements of phenotypic hyperexcitability. Indeed, elevated extracellular K^+ has been shown to alter the neuronal excitability and neural circuit stability in a mouse model of SCZ (Crabtree et al., 2017). Thus, the decreased K^+ uptake of SCZ glia may be a significant contributor to SCZ pathogenesis, especially in regards to those schizophrenic phenotypes associated with hyperexcitability and seizure disorders, which would be potentiated in the setting of disrupted potassium homeostasis.

We next established that the upregulated REST in SCZ glia appears both necessary and sufficient for their suppression of both KCN gene expression and potassium uptake. REST, as a transcriptional repressor, regulates neural gene expression in both neurons and glia (Bruce et al., 2004; Dewald et al., 2011). In broad terms, REST represses neural genes through its recruitment of CoREST and mSIN3a, the complex of which further recruits HDAC1/2 and methyltransferase G9a to promote concurrent histone deacetylation and methylation, which together serve to block transcription (Hirabayashi and Gotoh, 2010). As such, the misdirected upregulation of REST inhibits KCN gene expression and thereby contributes to the disease phenotype of those disorders associated with dysregulated potassium homeostasis and its attendant neuronal hyperexcitability. For instance, upregulated REST in peripheral sensory neurons induces the downregulation of KCNQ2, which in turn potentiates the hyperexcitability of sensory neurons and hence the maintenance of neuropathic pain (Rose et al., 2011). REST similarly represses KCNQ3 gene expression, and the downregulation of KCNQ3 by REST provokes neuronal hyperexcitability in specific neonatal epilepsies (Mucha et al., 2010).

Furthermore, REST is involved in SCZ through its modulation of miR137 (Warburton et al., 2015), which regulates multiple SCZ-associated genes, including CACNA1C, TCF4, and ANK3 (Kwon et al., 2013; Schizophrenia Psychiatric Genome-Wide Association Study (GWAS) Consortium, 2011). REST has been reported to be highly expressed in postmortem brain tissues from patients with SCZ (Loe-Mie et al., 2010). Other investigators have reported that REST can repress the expression of potassium-channel-associated genes (Bruce et al., 2004) and can suppress oligodendroglial differentiation within the glial lineage (Dewald et al., 2011). We thus hypothesized that pathologically high levels of REST might repress K^+-transporter- and channel-associated gene expression, and thereby decrease K^+ uptake, in SCZ-derived glia. This would be expected to lead to high interstitial K^+ and hence to relative neuronal hyperexcitability and network desynchronization. That said, the role of REST in disordered glial potassium homeostasis has not hitherto been reported. Our data suggest the likelihood that some fraction of schizophrenic patients might suffer high interstitial K^+ levels as a function of diminished glial potassium uptake. This would be expected to yield neuronal hyperexcitability as has been reported in Huntington's disease, another disorder characterized by glial KCN dysfunction (Benraiss et al., 2016). As such, our observation of a REST-dependent impairment of K^+ uptake by SCZ-derived glia suggests that REST might be an effective target for the treatment of SCZ. In that regard, several REST-targeted drugs have been developed for epilepsy and Huntington's disease, including valproic acid and X5050 (Charbord et al., 2013; Gräff and Tsai, 2013); our data suggest that these agents may have therapeutic utility in SCZ as well.

Thus, our data reveal the defective differentiation into astrocytes by SCZ GPCs, the potential reversibility of that defect by SMAD4 KD, and the differentiation-coupled, REST-dependent suppression of KCN gene expression and concomitant defective uptake of K^+ by SCZ glia. The resultant deficiencies in synaptic potassium homeostasis may be expected to significantly lower neuronal firing thresholds while accentuating network desynchronization (Benraiss et al., 2016). As such, one might expect that positive modulators of glial K^+ uptake may have real value in the treatment of SCZ (Calcaterra et al., 2016; He et al., 2013; Rahmanzadeh et al., 2017). Together, these findings identify a causal contribution of astrocytic pathology to the neuronal dysfunction of SCZ and in so doing suggest a set of tractable molecular targets for its treatment.

STAR★METHODS

Detailed methods are provided in the online version of this paper and include the following:

- KEY RESOURCES TABLE
- CONTACT FOR REAGENT AND RESOURCE SHARING
- EXPERIMENTAL MODEL AND SUBJECT DETAILS
  - Patient **identification, protection and sampling**
  - Cell sources and lines

SUPPLEMENTAL INFORMATION

Supplemental Information can be found online at https://doi.org/10.1016/j.celrep.2019.05.088.

ACKNOWLEDGMENTS

This work is supported by NIMH grants R01MH104701 and R01MH099578, the Novo Nordisk Foundation, the Lundbeck Foundation, the Dr. Miriam and Sheldon G. Adelson Medical Research Foundation, and the G. Harold and Leila Y. Mathers Charitable Foundation. We thank Lorenz Studer (Memorial Sloan Kettering) for the C27 hiPSC cell line and Didier Trono for the psPAX2 lentiviral vector. All genomic data have been deposited to GEO: GSE86906.

AUTHOR CONTRIBUTIONS

Z.L. performed all primary experiments; M.O., N.P.T.H., and R.F. performed the genomic and methylomic analyses; J.B. and Z.L. prepared the GPCs used in the study; D.C.-M. assisted Z.L. with cytometry and sorting; A.B. designed and assisted Z.L. in making the overexpression and KD viruses; M.N. and M.S.W. assisted in data analysis; R.L.F. and P.J.T. prepared the SCZ and CTR iPSCs; and S.A.G. designed the study, analyzed the data, and wrote the manuscript.

DECLARATION OF INTERESTS

The authors declare no competing interests in regards to this study. Regarding other, non-overlapping studies, Dr. Goldman is a co-founder and officer of Oscine Corp., a cell therapy company, and Drs. Goldman and Windrem are co-inventors on US and EU patents describing human glial chimeric mice and their use in modeling glial disorders. None of the other authors have any known conflicts of interest in regards to this work.

Received: December 22, 2018
Revised: April 4, 2019
Accepted: May 22, 2019
Published: June 25, 2019

REFERENCES

Aberg, K., Saetre, P., Lindholm, E., Ekholm, B., Pettersson, U., Adolfsson, R., and Jazin, E. (2006). Human QKI, a new candidate gene for schizophrenia involved in myelination. Am. J. Med. Genet. Part B *141B*, 84–90.

Allen, N.C., Bagade, S., McQueen, M.B., Ioannidis, J.P.A., Kavvoura, F.K., Khoury, M.J., Tanzi, R.E., and Bertram, L. (2008). Systematic meta-analyses and field synopsis of genetic association studies in schizophrenia: the SzGene database. Nat. Genet. *40*, 827–834.

Aryee, M.J., Jaffe, A.E., Corrada-Bravo, H., Ladd-Acosta, C., Feinberg, A.P., Hansen, K.D., and Irizarry, R.A. (2014). Minfi: a flexible and comprehensive Bioconductor package for the analysis of Infinium DNA methylation microarrays. Bioinformatics *30*, 1363–1369.

Benraiss, A., Wang, S., Herrlinger, S., Li, X., Chandler-Militello, D., Mauceri, J., Burm, H.B., Toner, M., Osipovitch, M., Jim Xu, Q., et al. (2016). Human glia can both induce and rescue aspects of disease phenotype in Huntington disease. Nat. Commun. *7*, 11758.

Blanco-Suárez, E., Caldwell, A.L., and Allen, N.J. (2017). Role of astrocyte-synapse interactions in CNS disorders. J. Physiol. *595*, 1903–1916.

Bøttger, P., Glerup, S., Gesslein, B., Illarionova, N.B., Isaksen, T.J., Heuck, A., Clausen, B.H., Füchtbauer, E.M., Gramsbergen, J.B., Gunnarson, E., et al. (2016). Glutamate-system defects behind psychiatric manifestations in a familial hemiplegic migraine type 2 disease-mutation mouse model. Sci. Rep. *6*, 22047.

Brazil, D.P., Church, R.H., Surae, S., Godson, C., and Martin, F. (2015). BMP signalling: agony and antagony in the family. Trends Cell Biol. *25*, 249–264.

Bruce, A.W., Donaldson, I.J., Wood, I.C., Yerbury, S.A., Sadowski, M.I., Chapman, M., Göttgens, B., and Buckley, N.J. (2004). Genome-wide analysis of repressor element 1 silencing transcription factor/neuron-restrictive silencing factor (REST/NRSF) target genes. Proc. Natl. Acad. Sci. USA *101*, 10458–10463.

Brzustowicz, L.M., Hodgkinson, K.A., Chow, E.W., Honer, W.G., and Bassett, A.S. (2000). Location of a major susceptibility locus for familial schizophrenia on chromosome 1q21-q22. Science *288*, 678–682.

Calcaterra, N.E., Hoeppner, D.J., Wei, H., Jaffe, A.E., Maher, B.J., and Barrow, J.C. (2016). Schizophrenia-Associated hERG channel Kv11.1-3.1 Exhibits a Unique Trafficking Deficit that is Rescued Through Proteasome Inhibition for High Throughput Screening. Sci. Rep. *6*, 19976.

Chambers, S.M., Fasano, C.A., Papapetrou, E.P., Tomishima, M., Sadelain, M., and Studer, L. (2009). Highly efficient neural conversion of human ES and iPS cells by dual inhibition of SMAD signaling. Nat. Biotechnol. *27*, 275–280.

Charbord, J., Poydenot, P., Bonnefond, C., Feyeux, M., Casagrande, F., Brinon, B., Francelle, L., Aurégan, G., Guillermier, M., Cailleret, M., et al. (2013). High throughput screening for inhibitors of REST in neural derivatives of human embryonic stem cells reveals a chemical compound that promotes expression of neuronal genes. Stem Cells *31*, 1816–1828.

Christopherson, K.S., Ullian, E.M., Stokes, C.C., Mullowney, C.E., Hell, J.W., Agah, A., Lawler, J., Mosher, D.F., Bornstein, P., and Barres, B.A. (2005). Thrombospondins are astrocyte-secreted proteins that promote CNS synaptogenesis. Cell *120*, 421–433.

Chung, W.S., Clarke, L.E., Wang, G.X., Stafford, B.K., Sher, A., Chakraborty, C., Joung, J., Foo, L.C., Thompson, A., Chen, C., et al. (2013). Astrocytes mediate synapse elimination through MEGF10 and MERTK pathways. Nature *504*, 394–400.

Clarke, L.E., and Barres, B.A. (2013). Emerging roles of astrocytes in neural circuit development. Nat. Rev. Neurosci. *14*, 311–321.

Coppi, E., Maraula, G., Fumagalli, M., Failli, P., Cellai, L., Bonfanti, E., Mazzoni, L., Coppini, R., Abbracchio, M.P., Pedata, F., and Pugliese, A.M. (2013). UDP-glucose enhances outward K(+) currents necessary for cell differentiation and stimulates cell migration by activating the GPR17 receptor in oligodendrocyte precursors. Glia *61*, 1155–1171.

Crabtree, G.W., Sun, Z., Kvajo, M., Broek, J.A., Fénelon, K., McKellar, H., Xiao, L., Xu, B., Bahn, S., O'Donnell, J.M., and Gogos, J.A. (2017). Alteration of neuronal excitability and short-term synaptic plasticity in the prefrontal cortex of a mouse model of mental illness. J. Neurosci. *37*, 4158–4180.

Dewald, L.E., Rodriguez, J.P., and Levine, J.M. (2011). The RE1 binding protein REST regulates oligodendrocyte differentiation. J. Neurosci. *31*, 3470–3483.

Fields, R.D. (2008). White matter in learning, cognition and psychiatric disorders. Trends Neurosci. *31*, 361–370.

Fromer, M., Roussos, P., Sieberts, S.K., Johnson, J.S., Kavanagh, D.H., Perumal, T.M., Ruderfer, D.M., Oh, E.C., Topol, A., Shah, H.R., et al. (2016). Gene expression elucidates functional impact of polygenic risk for schizophrenia. Nat. Neurosci. *19*, 1442–1453.

Gamba, G., and Friedman, P.A. (2009). Thick ascending limb: the Na(+):K(+):2Cl (-) co-transporter, NKCC2, and the calcium-sensing receptor, CaSR. Pflugers Arch. *458*, 61–76.

Goldman, S.A., and Kuypers, N.J. (2015). How to make an oligodendrocyte. Development *142*, 3983–3995.

Goudriaan, A., de Leeuw, C., Ripke, S., Hultman, C.M., Sklar, P., Sullivan, P.F., Smit, A.B., Posthuma, D., and Verheijen, M.H. (2014). Specific glial functions contribute to schizophrenia susceptibility. Schizophr. Bull. *40*, 925–935.

Gräff, J., and Tsai, L.H. (2013). The potential of HDAC inhibitors as cognitive enhancers. Annu. Rev. Pharmacol. Toxicol. *53*, 311–330.

Hata, A., and Chen, Y.G. (2016). TGF-β Signaling from Receptors to Smads. Cold Spring Harb. Perspect. Biol. *8*, a022061.

He, F.Z., McLeod, H.L., and Zhang, W. (2013). Current pharmacogenomic studies on hERG potassium channels. Trends Mol. Med. *19*, 227–238.

Herhaus, L., and Sapkota, G.P. (2014). The emerging roles of deubiquitylating enzymes (DUBs) in the TGFβ and BMP pathways. Cell. Signal. *26*, 2186–2192.

Hirabayashi, Y., and Gotoh, Y. (2010). Epigenetic control of neural precursor cell fate during development. Nat. Rev. Neurosci. *11*, 377–388.

Hu, J., Wang, D., Li, J., Jing, G., Ning, K., and Xu, J. (2014). Genome-wide identification of transcription factors and transcription-factor binding sites in oleaginous microalgae Nannochloropsis. Sci. Rep. *4*, 5454.

Kohyama, J., Sanosaka, T., Tokunaga, A., Takatsuka, E., Tsujimura, K., Okano, H., and Nakashima, K. (2010). BMP-induced REST regulates the establishment and maintenance of astrocytic identity. J. Cell Biol. *189*, 159–170.

Kwon, E., Wang, W., and Tsai, L.H. (2013). Validation of schizophrenia-associated genes CSMD1, C10orf26, CACNA1C and TCF4 as miR-137 targets. Mol. Psychiatry *18*, 11–12.

Larsen, B.R., Assentoft, M., Cotrina, M.L., Hua, S.Z., Nedergaard, M., Kaila, K., Voipio, J., and MacAulay, N. (2014). Contributions of the Na^+/K^+-ATPase, NKCC1, and Kir4.1 to hippocampal K^+ clearance and volume responses. Glia *62*, 608–622.

Lee, Y.H., Kim, J.H., and Song, G.G. (2013). Pathway analysis of a genome-wide association study in schizophrenia. Gene *525*, 107–115.

Lesage, F., Guillemare, E., Fink, M., Duprat, F., Heurteaux, C., Fosset, M., Romey, G., Barhanin, J., and Lazdunski, M. (1995). Molecular properties of neuronal G-protein-activated inwardly rectifying K+ channels. J. Biol. Chem. *270*, 28660–28667.

Loe-Mie, Y., Lepagnol-Bestel, A.M., Maussion, G., Doron-Faigenboim, A., Imbeaud, S., Delacroix, H., Aggerbeck, L., Pupko, T., Gorwood, P., Simonneau, M., and Moalic, J.M. (2010). SMARCA2 and other genome-wide supported schizophrenia-associated genes: regulation by REST/NRSF, network organization and primate-specific evolution. Hum. Mol. Genet. *19*, 2841–2857.

Macaulay, N., and Zeuthen, T. (2012). Glial K^+ clearance and cell swelling: key roles for cotransporters and pumps. Neurochem. Res. *37*, 2299–2309.

Maldonado, P.P., Vélez-Fort, M., Levavasseur, F., and Angulo, M.C. (2013). Oligodendrocyte precursor cells are accurate sensors of local K+ in mature gray matter. J. Neurosci. *33*, 2432–2442.

Marshall, C.R., Howrigan, D.P., Merico, D., Thiruvahindrapuram, B., Wu, W., Greer, D.S., Antaki, D., Shetty, A., Holmans, P.A., Pinto, D., et al.; Psychosis Endophenotypes International Consortium; CNV and Schizophrenia Working Groups of the Psychiatric Genomics Consortium (2017). Contribution of copy number variants to schizophrenia from a genome-wide study of 41,321 subjects. Nat. Genet. *49*, 27–35.

Molofsky, A.V., Krencik, R., Ullian, E.M., Tsai, H.H., Deneen, B., Richardson, W.D., Barres, B.A., and Rowitch, D.H. (2012). Astrocytes and disease: a neurodevelopmental perspective. Genes Dev. *26*, 891–907.

Mucha, M., Ooi, L., Linley, J.E., Mordaka, P., Dalle, C., Robertson, B., Gamper, N., and Wood, I.C. (2010). Transcriptional control of KCNQ channel genes and the regulation of neuronal excitability. J. Neurosci. *30*, 13235–13245.

O'Donovan, M.C., and Owen, M.J. (1999). Candidate-gene association studies of schizophrenia. Am. J. Hum. Genet. *65*, 587–592.

Onichtchouk, D., Chen, Y.G., Dosch, R., Gawantka, V., Delius, H., Massagué, J., and Niehrs, C. (1999). Silencing of TGF-beta signalling by the pseudoreceptor BAMBI. Nature *401*, 480–485.

Penzes, P., Cahill, M.E., Jones, K.A., VanLeeuwen, J.E., and Woolfrey, K.M. (2011). Dendritic spine pathology in neuropsychiatric disorders. Nat. Neurosci. *14*, 285–293.

Rahmanzadeh, R., Shahbazi, A., Ardakani, M.K., Mehrabi, S., Rahmanzade, R., and Joghataei, M.T. (2017). Lack of the effect of bumetanide, a selective NKCC1 inhibitor, in patients with schizophrenia: A double-blind randomized trial. Psychiatry Clin. Neurosci. *71*, 72–73.

Rajkowska, G., Miguel-Hidalgo, J.J., Makkos, Z., Meltzer, H., Overholser, J., and Stockmeier, C. (2002). Layer-specific reductions in GFAP-reactive astroglia in the dorsolateral prefrontal cortex in schizophrenia. Schizophr. Res. *57*, 127–138.

Rangroo Thrane, V., Thrane, A.S., Wang, F., Cotrina, M.L., Smith, N.A., Chen, M., Xu, Q., Kang, N., Fujita, T., Nagelhus, E.A., and Nedergaard, M. (2013). Ammonia triggers neuronal disinhibition and seizures by impairing astrocyte potassium buffering. Nat. Med. *19*, 1643–1648.

Rose, K., Ooi, L., Dalle, C., Robertson, B., Wood, I.C., and Gamper, N. (2011). Transcriptional repression of the M channel subunit Kv7.2 in chronic nerve injury. Pain *152*, 742–754.

Sawa, A., and Snyder, S.H. (2002). Schizophrenia: diverse approaches to a complex disease. Science *296*, 692–695.

Schizophrenia Psychiatric Genome-Wide Association Study (GWAS) Consortium. (2011). Genome-wide association study identifies five new schizophrenia loci. Nat. Genet *43*, 969–976.

Schizophrenia Working Group of the Psychiatric Genomics Consortium (2014). Biological insights from 108 schizophrenia-associated genetic loci. Nature *511*, 421–427.

Seifert, G., Schilling, K., and Steinhäuser, C. (2006). Astrocyte dysfunction in neurological disorders: a molecular perspective. Nat. Rev. Neurosci. *7*, 194–206.

Sim, F.J., Lang, J.K., Waldau, B., Roy, N.S., Schwartz, T.E., Pilcher, W.H., Chandross, K.J., Natesan, S., Merrill, J.E., and Goldman, S.A. (2006). Complementary patterns of gene expression by human oligodendrocyte progenitors and their environment predict determinants of progenitor maintenance and differentiation. Ann. Neurol. *59*, 763–779.

Sim, F.J., McClain, C.R., Schanz, S.J., Protack, T.L., Windrem, M.S., and Goldman, S.A. (2011). CD140a identifies a population of highly myelinogenic, migration-competent and efficiently engrafting human oligodendrocyte progenitor cells. Nat. Biotechnol. *29*, 934–941.

Singh, S.K., Stogsdill, J.A., Pulimood, N.S., Dingsdale, H., Kim, Y.H., Pilaz, L.J., Kim, I.H., Manhaes, A.C., Rodrigues, W.S., Jr., Pamukcu, A., et al. (2016). Astrocytes Assemble Thalamocortical Synapses by Bridging NRX1α and NL1 via Hevin. Cell *164*, 183–196.

Smedemark-Margulies, N., Brownstein, C.A., Vargas, S., Tembulkar, S.K., Towne, M.C., Shi, J., Gonzalez-Cuevas, E., Liu, K.X., Bilguvar, K., Kleiman, R.J., et al. (2016). A novel de novo mutation in ATP1A3 and childhood-onset schizophrenia. Cold Spring Harb. Mol. Case Stud. *2*, a001008.

Somers, A., Jean, J.C., Sommer, C.A., Omari, A., Ford, C.C., Mills, J.A., Ying, L., Sommer, A.G., Jean, J.M., Smith, B.W., et al. (2010). Generation of transgene-free lung disease-specific human induced pluripotent stem cells using a single excisable lentiviral stem cell cassette. Stem Cells *28*, 1728–1740.

Steffek, A.E., McCullumsmith, R.E., Haroutunian, V., and Meador-Woodruff, J.H. (2008). Cortical expression of glial fibrillary acidic protein and glutamine synthetase is decreased in schizophrenia. Schizophr. Res. *103*, 71–82.

Swarts, H.G., Weigand, K.M., Venselaar, H., van den Maagdenberg, A.M., Russel, F.G., and Koenderink, J.B. (2013). Familial hemiplegic migraine mutations affect Na,K-ATPase domain interactions. Biochim. Biophys. Acta *1832*, 2173–2179.

Takahashi, N., and Sakurai, T. (2013). Roles of glial cells in schizophrenia: possible targets for therapeutic approaches. Neurobiol. Dis. *53*, 49–60.

Takahashi, K., Tanabe, K., Ohnuki, M., Narita, M., Ichisaka, T., Tomoda, K., and Yamanaka, S. (2007). Induction of pluripotent stem cells from adult human fibroblasts by defined factors. Cell *131*, 861–872.

Takahashi, N., Sakurai, T., Bozdagi-Gunal, O., Dorr, N.P., Moy, J., Krug, L., Gama-Sosa, M., Elder, G.A., Koch, R.J., Walker, R.H., et al. (2011a). Increased expression of receptor phosphotyrosine phosphatase-β/ζ is associated with molecular, cellular, behavioral and cognitive schizophrenia phenotypes. Transl. Psychiatry *1*, e8.

Takahashi, N., Sakurai, T., Davis, K.L., and Buxbaum, J.D. (2011b). Linking oligodendrocyte and myelin dysfunction to neurocircuitry abnormalities in schizophrenia. Prog. Neurobiol. *93*, 13–24.

Tkachev, D., Mimmack, M.L., Ryan, M.M., Wayland, M., Freeman, T., Jones, P.B., Starkey, M., Webster, M.J., Yolken, R.H., and Bahn, S. (2003). Oligodendrocyte dysfunction in schizophrenia and bipolar disorder. Lancet *362*, 798–805.

Tong, X., Ao, Y., Faas, G.C., Nwaobi, S.E., Xu, J., Haustein, M.D., Anderson, M.A., Mody, I., Olsen, M.L., Sofroniew, M.V., and Khakh, B.S. (2014). Astrocyte Kir4.1 ion channel deficits contribute to neuronal dysfunction in Huntington's disease model mice. Nat. Neurosci. *17*, 694–703.

Verkhratsky, A., and Parpura, V. (2016). Astrogliopathology in neurological, neurodevelopmental and psychiatric disorders. Neurobiol. Dis. *85*, 254–261.

Verkhratsky, A., Nedergaard, M., and Hertz, L. (2015). Why are astrocytes important? Neurochem. Res. *40*, 389–401.

Voineskos, A.N., Felsky, D., Kovacevic, N., Tiwari, A.K., Zai, C., Chakravarty, M.M., Lobaugh, N.J., Shenton, M.E., Rajji, T.K., Miranda, D., et al. (2013). Oligodendrocyte genes, white matter tract integrity, and cognition in schizophrenia. Cereb. Cortex *23*, 2044–2057.

Wang, S., Bates, J., Li, X., Schanz, S., Chandler-Militello, D., Levine, C., Maherali, N., Studer, L., Hochedlinger, K., Windrem, M., and Goldman, S.A. (2013). Human iPSC-derived oligodendrocyte progenitor cells can myelinate and rescue a mouse model of congenital hypomyelination. Cell Stem Cell *12*, 252–264.

Wang, C., Aleksic, B., and Ozaki, N. (2015). Glia-related genes and their contribution to schizophrenia. Psychiatry Clin. Neurosci. *69*, 448–461.

Warburton, A., Breen, G., Rujescu, D., Bubb, V.J., and Quinn, J.P. (2015). Characterization of a REST-Regulated Internal Promoter in the Schizophrenia Genome-Wide Associated Gene MIR137. Schizophr. Bull. *41*, 698–707.

Welstead, G.G., Brambrink, T., and Jaenisch, R. (2008). Generating iPS cells from MEFS through forced expression of Sox-2, Oct-4, c-Myc, and Klf4. J. Vis. Exp. 2008, 734.

Westbrook, T.F., Hu, G., Ang, X.L., Mulligan, P., Pavlova, N.N., Liang, A., Leng, Y., Maehr, R., Shi, Y., Harper, J.W., and Elledge, S.J. (2008). SCFbeta-TRCP controls oncogenic transformation and neural differentiation through REST degradation. Nature *452*, 370–374.

Williams, M.R., Hampton, T., Pearce, R.K., Hirsch, S.R., Ansorge, O., Thom, M., and Maier, M. (2013). Astrocyte decrease in the subgenual cingulate and callosal genu in schizophrenia. Eur. Arch. Psychiatry Clin. Neurosci. *263*, 41–52.

Windrem, M.S., Osipovitch, M., Liu, Z., Bates, J., Chandler-Militello, D., Zou, L., Munir, J., Schanz, S., McCoy, K., Miller, R.H., et al. (2017). Human iPSC glial mouse chimeras reveal glial contributions to schizophrenia. Cell Stem Cell *21*, 195–208.e6.

Xia, M., Abazyan, S., Jouroukhin, Y., and Pletnikov, M. (2016). Behavioral sequelae of astrocyte dysfunction: focus on animal models of schizophrenia. Schizophr. Res25468180 *176*, 72–82..

Xie, L., Kang, H., Xu, Q., Chen, M.J., Liao, Y., Thiyagarajan, M., O'Donnell, J., Christensen, D.J., Nicholson, C., Iliff, J.J., et al. (2013). Sleep drives metabolite clearance from the adult brain. Science *342*, 373–377.

Yin, D.M., Chen, Y.J., Sathyamurthy, A., Xiong, W.C., and Mei, L. (2012). Synaptic dysfunction in schizophrenia. Adv. Exp. Med. Biol. *970*, 493–516.

Zhang, Y., and Barres, B.A. (2010). Astrocyte heterogeneity: an underappreciated topic in neurobiology. Curr. Opin. Neurobiol. *20*, 588–594.

Zou, X.Y., Yang, H.Y., Yu, Z., Tan, X.B., Yan, X., and Huang, G.T. (2012). Establishment of transgene-free induced pluripotent stem cells reprogrammed from human stem cells of apical papilla for neural differentiation. Stem Cell Res. Ther. *3*, 43.

STAR★METHODS

KEY RESOURCES TABLE

REAGENT or RESOURCE	SOURCE	IDENTIFIER
Antibodies		
Rabbit polyclonal anti-Nanog, 1:200	Millipore	Cat # AB9220; RRID: AB_570613
Mouse monoclonal anti-human TRA1-60, 1:200	Millipore	Cat # MAB4360; RRID: AB_2119183
Rabbit polyclonal anti-PAX6, 1:400	Covance Research Products Inc	Cat # PRB-278p; RRID: AB_291612
Rabbit monoclonal anti-PDGF Receptor alpha, clone D13C6, 1:300	Cell Signaling Technology	Cat #5241S; RRID: AB_10692773
Mouse monoclonal anti-human GFAP, clone SMI 21R, 1:500	Covance Research Products	Cat#SMI-21R-500; RRID: AB_509979
Mouse monoclonal anti-S100 beta, clone SH-B1, 1:500	Abcam	Cat #ab11178; RRID: AB_297817
Goat polyclonal anti-human SOX1, 1:200	R&D Systems	Cat # AF3369; RRID: AB_2239897
Donkey anti-mouse IgG (H+L) Alexa Fluor 594, 1:400	ThermoFisher Scientific	Cat # A-21203; RRID: AB_2535789
Donkey anti-mouse IgG (H+L) Alexa Fluor 488, 1:400	ThermoFisher Scientific	Cat #A-21202; RRID: AB_141607
Donkey anti-Rabbit IgG (H+L) Alexa Fluor 594, 1:400	ThermoFisher Scientific	Cat #A-21207; RRID: AB_141637
Donkey anti-Rabbit IgG (H+L) Alexa Fluor 488, 1:400	ThermoFisher Scientific	Cat #A-21206; RRID: AB_2535792
Donkey anti-Goat IgG (H+L) Alexa Fluor 594, 1:400	ThermoFisher Scientific	Cat #A-11058; RRID: AB_2534105
Mouse monoclonal anti-SSEA4 FITC Conjugate, 1:100	Life Technologies	Cat # MC-813-70; RRID: AB_528477
APC-conjugated mouse IgG1, Isotype Control, 1:10	Miltenyi Biotec	Cat#130-092-214; RRID: AB_871704
APC-mouse IgM, Isotype Control, 1:40	Miltenyi Biotec	Cat#130-093-176; RRID: AB_871720
Rat anti-mouse IgG2a+b, microbeads, 1:100	Miltenyi Biotec	Cat #130-047-201; RRID: AB_244356
Mouse anti-CD44 microbeads, 1:100	Miltenyi Biotec	Cat #130-095-194
APC-conjugated anti-CD133/1, 1:10	Miltenyi Biotec	Cat#130-090-826; RRID: AB_244340
Mouse monoclonal anti-CD140a. Unconjugated, 1:100	BD Biosciences	Cat #556001; RRID: AB_396285
PE-conjugated anti-CD140a, 1:10	BD Biosciences	Cat#556002; RRID: AB_396286
APC-conjugated anti-CD44, 1:10	Miltenyi Biotec	Cat #130-095-177; RRID: AB_10839563
PE-conj. anti-mouse IgG2a, isotype control, 1:10	BD PharMingen	Cat#555574; RRID: AB_395953
Chemicals, Peptides, and Recombinant Proteins		
Dulbecco's Modified Eagle Medium	Invitrogen	Cat #11965-092
Fetal Bovine Serum	Invitrogen	Cat #16000-044
Non-Essential Amino Acid	Invitrogen	Cat # 11140-050
Dulbecco's Modified Eagle Medium/Nutrient Mixture F-12	Invitrogen	Cat #11330-032
KnockOut Serum Replacement	Invitrogen	Cat #10828-028
FBS	VWR	Cat#16777-014
Donkey serum	Millipore	Cat#5058837
Goat serum	Invitrogen	Cat#16210-072
DPBS	Invitrogen	Cat# 14190-250
Thimerosal	Sigma	T5125
L-glutamine	Invitrogen	Cat #25030-081
Gelatin	Sigma	Cat#G1890-100G
2-Mercaptoethanol	Sigma	Cat #M7522
Saponin	Fluka Analytical	Cat#47036
B27 Supplement	Invitrogen	Cat #12587-010
N1 Supplement	Sigma	Cat # N6530
Selenite	Sigma	Cat #S9133
Progesterone	Sigma	Cat #P6149

(*Continued on next page*)

Continued

REAGENT or RESOURCE	SOURCE	IDENTIFIER
Rubidium-86	PerkinElmer	Cat#NEZ072001MC
Ouabain	Sigma	Cat # O3125
Bumetanide	R&D Systems	Cat #3108
Tertiapin	R&D Systems	Cat #1316
NaOH	Fisher Scientific	Cat#MSX0607H6
NaCl	Invitrogen	Cat#AM9760G
KCl	Invitrogen	Cat#AM9640G
CaCl2	Sigma	Cat#21108-500 g
vitamin C	Sigma	Cat#A4034-100G
NaHCO3	Sigma	Cat#S-8875
MgCl2	Sigma	Cat#M8266-IKG
NaH2PO4	Sigma	Cat#S3264-500G
Glucose	Sigma	Cat#G8769-100ML
Cocktail liquid	Fisher Scientific	Cat#509050575
N2 Supplement	Invitrogen	Cat #17502-048
bFGF	Sigma	Cat #F0291
bFGF	Invitrogen	Cat#13256-029
Collagenase	Invitrogen	Cat#17104-019
Dispase	Invitrogen	Cat#17105-041
Poly-ornithine	Sigma	Cat# P4957
Laminin	VWR	Cat#47743
Biotin	Sigma	Cat #B4639
dibutyryl cAMP	Sigma	Cat #D0260
Heparin	Fisher	Cat#NC9484621
IGF-1	R&D Systems	Cat #291-G1-050
Laminin	Corning	Cat#354232
NT3	R&D Systems	Cat #267-N3-025
PDGFaa	R&D Systems	Cat #221-AA-50
BMP4	PeproTech	Cat#AF-120-05ET
Accutase	Fisher Scientific	Cat# SCR005
Purmorphamine	Calbiochem	Cat #80603-730
Retinoic acid	Sigma	Cat #R2625
DMH1	Sigma	Cat#D8946-5MG
T3	Sigma	Cat #T5516-1MG
4% paraformaldehyde	Fisher Scientific	Cat#NC9245948
X-tremeGENE	Roche	Cat#06366236001
Doxycycline	Fisher Scientific	Cat#ICN19895510
Critical Commercial Assays		
RNeasy mini kit	QIAGEN	Cat#74104
QIAamp DNA micro kit	QIAGEN	Cat#56304
Taqman Reverse Transcription kit	Fisher Scientific	Cat#N8080234
BCA Protein Assay kit	Fisher Scientific	Cat#23227
Perkin Elmer LLC ULTIMA-GOLD LITERS	Fisher Scientific	Cat#509050575
Deposited Data		
All raw data	Mendeley data	https://doi.org/10.17632/wvnxgw7xzf.1
RNA expression data	GEO	accession number GEO: GSE86906
Data processing and analytic routines	Github	https://github.com/cbtncph/GoldmanetalSCZ2016

(*Continued on next page*)

Continued

REAGENT or RESOURCE	SOURCE	IDENTIFIER
Experimental Models: Cell Lines		
C27	L. Studer, SKI	N/A
CWRU8, female, age 10	P. Tesar, Case Western	N/A
CWRU208, male, age 25	P. Tesar, Case Western	N/A
CWRU22, male, age 26	P. Tesar, Case Western	N/A
CWRU29, male, age 12 (same person as line 30 and 31)	P. Tesar, Case Western	N/A
CWRU30, male, age 12 (same person as line 29 and 31)	P. Tesar, Case Western	N/A
CWRU31, male, age 12 (same person as line 29 and 30)	P. Tesar, Case Western	N/A
CWRU37, female, age 32	P. Tesar, Case Western	N/A
CWRU51 male, age 16 (same person as line 52)	P. Tesar, Case Western	N/A
CWRU52 male, age 16 (same person as line 51)	P. Tesar, Case Western	N/A
CWRU164, female, age 14	P. Tesar, Case Western	N/A
CWRU193, female, age 15	P. Tesar, Case Western	N/A
293T	Fisher Scientific	Cat# R70007
Oligonucleotides		
ShRNA targeting sequence: REST #1: GCAGTGGCAACATTGGAATGG; #2: CGGCTACAATACTAATCGA	This paper	N/A
ShRNA targeting sequence: SMAD4 #1: TGGTCAGCCAGCTACTTAC; #2: ATGAATATGACTCACTTCT	GE Healthcare	Cat#V3SH11252
shScramble: AAGTTGCAAATCGCGTCTCTA	This paper	N/A
Recombinant DNA		
human cDNA of REST	Westbrook et al., 2008	Addgene plasmid #41903
human cDNA of SMAD4	GE Healthcare	Cat#MHS6278
Plasmid: pTANK-EF1a-coGFP-P2a-Puro- WPRE	This paper	N/A
Plasmid: pTANK-EF1a-IRES-mCherry-WPRE	Benraiss et al., 2016	N/A
Bacterial and Virus Strains		
TOP10 Chemically Competent E.coli	Invitrogen	Cat#K4600-01
Software and Algorithms		
Photoshop CS6	Adobe	N/A
Illustrator CS6	Adobe	N/A
FlowJo	TreeStar	N/A
Ingenuity Pathway Analysis	QIAGEN	https://www.qiagenbioinformatics.com/products/ingenuity-pathway-analysis/
TRANSFAC	Genexplain	https://www.genexplain.com/transfac/
minfi (version 1.28.2)	Aryee et al., 2014	https://bioconductor.org/packages/release/bioc/html/minfi.html
Other		
Agilent Bioanalyzer	Agilent	N/A
BD FACS Aria IIIU	BD Biosciences	N/A
Ultracentrifuge	Beckman	Cat #L8-70
Becksman Coulter	Beckman	Cat #LS6500
Hemocytometer	Fisher Scientific	Cat#02-671-54
HiSeq 2500	Illumina	N/A
Nanodrop 1000 spectrophotometer	Nanodrop	N/A
Olympus IX71 Inverted Microscope	Olympus	N/A
QuantStudio 12K Flex Real-Time PCR system	Applied Biosystems	N/A
Orca-R2 Digital CCD Camera	Hamamatsu	Cat #C10600-10B

CONTACT FOR REAGENT AND RESOURCE SHARING

Further information and requests for resources and reagents should be directed to and will be fulfilled by the lead contact, Steve Goldman. He may be contacted at: steven_goldman@urmc.rochester.edu or goldman@sund.ku.dk.

EXPERIMENTAL MODEL AND SUBJECT DETAILS

Patient identification, protection and sampling

Patients from which these lines were derived were diagnosed with disabling degrees of schizophrenia with onset in early adolescence; all patients and their guardians were consented/assented by a child and adolescent psychiatrist working under the supervision of one of us (RLF), and under the auspices of an approved protocol of the University Hospitals Case Medical Center Institutional Review Board, blinded as to subsequent line designations. No study investigators had access to patient identifiers.

Cell sources and lines

Schizophrenia-derived iPSC lines were produced from subjects with childood-onset schizophrenia, and control lines were produced from age- and gender-appropriate control subjects; all iPSC lines were derived as previously reported (Windrem et al., 2017). An additonal control line (C27; Wang et al., 2013) was graciously provided by Dr. Lorenz Studer (Memorial Sloan Kettering). Control-derived lines included: CWRU-22 (26 year-old male), −37 (32 year-old female), −208 (25 year-old male), and C27; SCZ-derived lines included CWRU-8 (10 year-old female), −51(16 year-old male), −52 (16 year-old male), −193 (15 year-old female), −164 (14 year-old female), −29 (12 year-old male), −30 (12 year-old male), and −31 (12 year-old male) (Windrem et al., 2017; see Table S1). CWRU-51/52 and CWRU-29/30/31 comprised different lines from the same patients, and were assessed to estimate inter-line variability from single patients. All iPSCs were generated from fibroblasts by retroviral expression of Cre-excisable Yamanaka factors (Oct4, Sox2, Klf4, c-Myc) (Takahashi et al., 2007), with validation of pluripotency and karyotypic stability as described (Windrem et al., 2017).

METHOD DETAILS

hiPSC culture and passage

hiPSCs were cultured on irradiated mouse embryonic fibroblasts (MEFs), in 0.1% gelatin (Sigma G1890-100G)-coated 6-well plates with 1-1.2 million cells/well in hESC medium (*see below*) supplemented with 10 ng/ml bFGF (Invitrogen, 13256-029). Media changes were performed daily, and cells passaged at 80% confluence, after 4-7 days of culture. For hiPSC passage, cells were first incubated with 1ml collagenase (Invitrogen, 17104-019) at 37°C for 3-5 minutes, and then cells were transferred into a 15 mL tube for centrifuge with 3 minutes. The pellet was re-suspended with ES medium with bFGF, and was plated onto new irradiated MEFs at 1:3-1:4.

GPC and astrocytic generation from hiPSCs

When hiPSCs reached 80% confluence, they were incubated with 1 mL Dispase (Invitrogen, 17105-041) to permit the generation of embryoid bodies (Ebs); these were cultured in ES medium without bFGF for 5 days. At DIV6, Ebs were plated onto poly-ornithine (Sigma, P4957) and laminin (VWR, 47743)-coated dishes, and cultured in neural induction media (NIM; *see below*) (Wang et al., 2013), supplemented with 20 ng/ml bFGF, 2 μg/ml heparin and 10 μg/ml laminin for 10 days.

At DIV 25, the Ebs were gently scraped with a 2 mL glass pipette, then cultured in NIM plus 1 μM purmorphamine (Calbiochem, 80603-730) and 0.1 μM RA (Sigma, R2625). At DIV 33, NPCs appeared and were serially switched to NIM with 1 μM purmorphamine and 10 ng/ml bFGF for 7 days, followed by glial induction medium (GIM) (Wang et al., 2013), with 1 μM purmorphamine for another 15 days. At DIV 56, the resultant glial spheres were mechanically cut with microsurgical blades under a dissection microscope, and switched to GIM with 10 ng/ml PDGF, 10 ng/ml IGF, and 10 ng/ml NT3, with media changes every 2 days. At DIV 80-100, CTR GPCs were cultured with 10 ng/ml BMP4 (PeproTech, AF-120-05ET) and 0.5 μM DMH1 (Sigma, D8946-5MG) for 2 weeks, and SCZ GPCs were transduced with lentiviral-SMAD4-shRNAi for 2 weeks, both of which were used for validation of REST and K^+ transport gene expression. At DIV 150-180, GPCs were incubated with mouse anti-CD44 microbeads (1:50), and then incubated with rabbit anti-mouse IgG2a+b micro-beads (1:100) and further sorted by magnetic cell sorting (MACS) with a magnetic stand column. The $CD44^+$ cells were then matured as astrocytes in M41 supplemented with 10% FBS (VWR, 16777-014) plus 20 ng/mL BMP4 for 4 weeks.

Media recipes are listed in Table S2 (hESC and neural media) and S3 (Glial and Astrocyte induction media).

FACS/MACS sorting

Cells were incubated with Accutase (Fisher Scientific, SCR005) for 5 minutes at 37°C to obtain a single cell suspension, and then spun down at 200RCF for 10 minutes. These GPCs were re-suspended in cold Miltenyi Wash buffer with primary antibody (phycoerythrin (PE)-conjugated mouse anti-CD140a, 1:50, for FACS; mouse anti-CD140a, 1:100, for MACS), and incubated on ice for 30 min, gently swirling every 10 minutes. After primary antibody incubation, these cells were then washed and either incubated with a secondary antibody (rabbit anti-mouse IgG2a+b micro-beads, 1:100) followed by sorting on a magnetic stand column for MACS, or directly

sorted by FACS on a FACSAria IIIu (Becton Dickinson). The sorted cells were counted and plated onto poly-ornithine- and laminin-coated 24-well plate for further experiments. Antibodies and dilutions used see Key Resources Table.

RT-PCR

Total RNA was extracted from cell lines with miRNeasy mini kit (QIAGEN, 217004), and then was reversely transcribed into cDNA with Taqman Reverse Transcription kit (Fisher Scientific, N8080234). The relative expression of mRNA was measured by the Bio-RAD S6048, which was further normalized to the expression of 18S mRNA.

The primer sequences are listed in Table S4.

Methylation

DNA was extracted from iPSC lines with the QIAamp DNA micro kit (QIAGEN, 56304), and then whole genome methylation analysis was performed using Illumina Methylation Epic arrays; this was done at the UCLA Neuroscience Genomics Core. Raw data from Intensity Data (IDAT) files were imported into R and normalized with the preprocessQuantile function from the package minfi (Aryee et al., 2014). Probes with poor quality signal were eliminated based on set threshold of detection p values (> 0.01). Probes were also eliminated if they map to the sex chromosomes, to multiple genomic locations, or if they contain single nucleotide polymorphisms at the CpG site. Following preprocessing, samples were assessed by principal component analysis (native R functions, https://www.R-project.org) based on their features of methylated intensities (M-values). To determine if a covariate (sex, age, cell line, etc.) could explain variation in our samples' methylation landscape, a linear regression model was fit for covariates and each principal component. Covariates with significant p values (< 0.05) were highlighted, indicating meaningful relationship between changes in the covariate (predictor variable) and changes in the principal component values (response variable).

In vitro immunocytochemistry

Cells were first fixed with 4% paraformaldehyde for 5 minutes at room temperature. After washing with D-PBS (Invitrogen, 14190-250) with thimerosal (Sigma, T5125) for 3 times, cells were penetrated with 0.1% saponin (Fluka Analytical, 47036) plus 1% of either goat or donkey serum for 15 minutes at room temperature. Cells were further blocked with 5% of either goat or donkey serum plus 0.05% saponin for 15 minutes at RT. After incubation with primary antibodies at 4°C overnight, the cells were incubated with secondary antibodies for 30 min at RT. The counts of immunofluorescent cells were taken from 10 random fields per each replicate, and each sample had three replicates.

Antibodies and dilutions used see Key Resources Table.

Molecular cloning and viral construction

REST shRNAs of human REST (target sequences: GCAGTGGCAACATTGGAATGG or CGGCTACAATACTAATCGA) were cloned into the vector pTANK-EF1α-CoGFP-Puro-WPRE immediately downstream puromycin. The human cDNAs encoding REST (a gift of Stephen Elledge, Addgene 41903) (Westbrook et al., 2008) and SMAD4 (GE Healthcare, MHS6278) were cloned downstream of the EF1α promoter in pTANK-EF1a-IRES-mCherry-WPRE (Benraiss et al., 2016). The lentiviral vector allowed for expression of REST and SMAD4 in tandem with the reporter mCherry. *SMAD4* Doxycycline-inducible shRNAs of human SMAD4 (Gene target sequence: TGGTCAGCCAGCTACTTAC or ATGAATATGACTCACTTCT) in pSMART-TRE3G-EGFP-Puro-WPRE were ordered from GE Healthcare (V3SH11252). *BAMBI* The human shRNA and cDNA of BAMBI were generated previously (Sim et al., 2006). The final constructs were validated for the correct insertion by sequencing. The plasmids were then co-transfected with pLP-VSV (Invitrogen, K497500) and psPAX2 (a gift from Didier Trono, Addgene 12260) into 293FT cells (Fisher Scientific, R70007) through X-tremeGENE (Roche, 06366236001) for lentiviral generation. The supernatants of 293T cells were then collected and spun at 76000 RCF for 3 hr to concentrate virus (Beckman L8-70, Ultracentrifuge). A 10-fold serial dilution of virus was then prepared and transduced into 293T cells, and fluorescent colonies counted to estimate viral titer.

Cell transduction

$CD140a^+$ hGPCs were isolated by MACS and then transduced with either lenti-TRE3G-SMAD4-shRNAi or lenti-EF1α-BAMBI-shRNAi, or their respective scrambled control viruses, MACS-sorted $CD44^+$ cells were transduced with either lenti-EF1α-REST-shRNAi or control virus, each at 1 MOI (multiplicities of infection) for 4 hours. Both lenti-EF1α-REST-shRNAi and lenti-EF1a-BAMBI-shRNAi efficiently inhibited the expression of their target genes (Figures S3 and S6A). Cells infected with lenti-TRE3G-SMAD4-shRNAi were treated with 0.5 μg/ml doxycycline (Fisher, CN19895510) beginning 4 days after viral infection; this was maintained for 1 week prior to experiment initiation; during this period, the cells were maintained in glial induction media. Under doxycycline, SMAD4 mRNA expression fell to < 30% of control; no inhibition was noted in the absence of doxycycline (Figures S4A–S4C).

Potassium uptake

Astrocytes were plated onto poly-ornithine- and laminin-coated 24-well plates with 30,000 cells/well. For the potassium uptake assay, astrocytes were incubated with ^{86}Rb (1.0-3.3uCi/well) for 15min, and then they were washed three time with ice-cold artificial cerebrospinal fluid (aCSF, 500uL/well). 0.5N NaOH (200uL/well) was put into each well for cell lysis, which was put into 5ml cocktail liquid (Ultima Gold, Fisher Scientific, 509050575) and measured by scintillation counter (Beckman Coulter, LS6500), and the results

were normalized to both total protein (BCA Protein Assay Kit, Fisher Scientific, 23227) and cell number (Hemocytometer, Fisher Scientific, 02-671-54). The aCSF solution contained (in mM): 124 NaCl, 2.5 KCl, 1.75 NaH_2PO_4, 2 $MgCl_2$, 2 $CaCl_2$, 0.04 vitamin C, 10 glucose and 26 $NaHCO_3$, pH 7.4.

QUANTIFICATION AND STATISTICAL ANALYSIS

Statistical parameters including the exact n, the center, dispersion, precision measures (mean ± SEM), and statistical significance are reported in the Figures and Figure Legends. All analyses were done with GraphPad PRISM 6 using one-way ANOVA and two tailed t test. Statistical significance was considered as P values less than 0.05. Significances were represented as $^{*}p < 0.05$, $^{**}p < 0.01$ and $^{***}p < 0.001$. Graphs and figures were made and assembled with Prism 6.

DATA AND SOFTWARE AVAILABILITY

All raw data have been uploaded to Mendeley data (https://data.mendeley.com), at https://data.mendeley.com/datasets/wvnxgw7xzf/draft?a=7661a24e-3cb1-4a1b-a072-ba6ac169d909.

Previous data processing and analysis routines from Windrem et al. (2017) are available from https://github.com/cbtncph/GoldmanetalSCZ2016, while the genomic data from that study have been deposited to GEO: GSE86906.